Electron and Ambipolar Transport in Organic Field-Effect Transistors

Jana Zaumseil and Henning Sirringhaus*

Cavendish Laboratory, JJ Thomson Avenue, Cambridge CB3 0HE, United Kingdom

Received July 31, 2006

Contents

* To whom correspondence should be addressed. E-mail: hs220@cam.ac.uk. Phone: +44 01223 337557. Fax: +44 01223 337706.

1. Introduction

Ever since the first field-effect transistors (FETs) based on polymer[1−3] and small molecule[4,5] semiconductors were reported, interest in this field has risen steadily for both technological and scientific reasons. In recent years, the number of publications on organic and polymer transistors has increased substantially (see Figure 1a). Organic FETs are technologically interesting because they could serve as the main component in cheap and flexible electronic circuits. Major possible applications are radio frequency identification (RF-ID) tags[6,7] and flexible displays.[8−12] Prototypes of these products have been demonstrated and are now getting close to being brought to the market.[13,14] Scientifically, organic semiconductors show interesting characteristics both similar to and different from known inorganic semiconductors, in particular amorphous silicon. The charge transport and emission properties of organic semiconductors have been under intense investigation for years, and field-effect transistors have proven to be a powerful tool for those efforts.

Common organic semiconductors are relatively wide band gap semiconductors with band gaps in the range of 2−3 eV. Methods for controlled doping of these materials are not well established, mainly because doping often requires the mixing of a redox active small molecular dopant into the organic semiconductor host, which can be mobile under applied electrical fields during device operation.[15−17] Therefore, in most applications, organic semiconductors are not intentionally doped and are used in their as-synthesized form. State-of-the-art methods for the synthesis and purification of polymer semiconductors are capable of controlling the concentration of impurities left over from the synthesis to ppm levels.[18,19] For small molecules, high chemical purity can be achieved using techniques such as vacuum sublimation.[20] Therefore, for many materials, even unintentional extrinsic doping levels are low enough to consider these materials as intrinsic semiconductors.

When incorporating these intrinsic organic semiconductors into field-effect transistor configurations—most commonly, thin-film transistors (TFTs)—to evaluate their charge transport characteristics in combination with a particular gate dielectric such as SiO_2, many of these materials exhibit hole accumulation behavior for negative applied gate voltages. However, when the gate voltage polarity is reversed to positive values, the formation of an electron accumulation layer is much less commonly observed. For many organic semiconductor-based FETs, only p-channel operation seems possible. For this reason, such materials have been called "p-type" organic semiconductors. Over the last 5 years, many groups have aimed to realize "n-type" organic FETs. This usually involved the synthesis of special organic semicon-

10.1021/cr0501543 CCC: $65.00
Published on Web 03/23/2007

Jana Zaumseil studied Chemistry at the University of Leipzig (Germany) and received her Diplom there in 2002. She then worked with Prof. John A. Rogers at Bell Laboratories on soft lithographic techniques and organic field-effect transistors before starting her doctoral work at the University of Cambridge under the supervision of Prof. Henning Sirringhaus in 2003. Her research focuses on ambipolar and light-emitting polymer field-effect transistors.

Henning Sirringhaus is the Hitachi Professor of Electron Device Physics at the Cavendish Laboratory. He has been working in the field of organic transistor devices since 1997. He has an undergraduate degree and a Ph.D. degree in physics from ETH Zürich (CH). From 1995–1996 he worked as a postdoctoral research fellow at Princeton University (U.S.A.) on a-Si TFTs for active-matrix liquid crystal displays. His current research interests include the charge transport physics of molecular and polymeric semiconductors, the development of printing-based nanopatterning techniques, and the use of scanning probe techniques for electrical characterization of functional nanostructures. He is co-founder and Chief Scientist of Plastic Logic Ltd., a technology start-up company commercializing printed organic transistor technology. He was awarded the Balzers Prize of the Swiss Physical Society in 1995 for his Ph.D. work on ballistic-electron-emission microscopy of epitaxial metal/semiconductor heterointerfaces, and the Mullard award of the Royal Society in 2003.

ductors with high electron affinities, comprising specific electron withdrawing groups. These were then called "n-type" organic semiconductors.

This classification has always been unsatisfactory, since it did not provide any insight into the reasons for the observed differences of transport properties of electrons and holes. It is also different from that used for most inorganic semiconductors, which are generally capable of conducting both electrons in the conduction band and holes in the valence band, and for which the distinction between p-type and n-type semiconductors is made entirely on the basis of extrinsic dopants being incorporated that are capable of inducing either holes in the valence band or electrons in the conduction band.

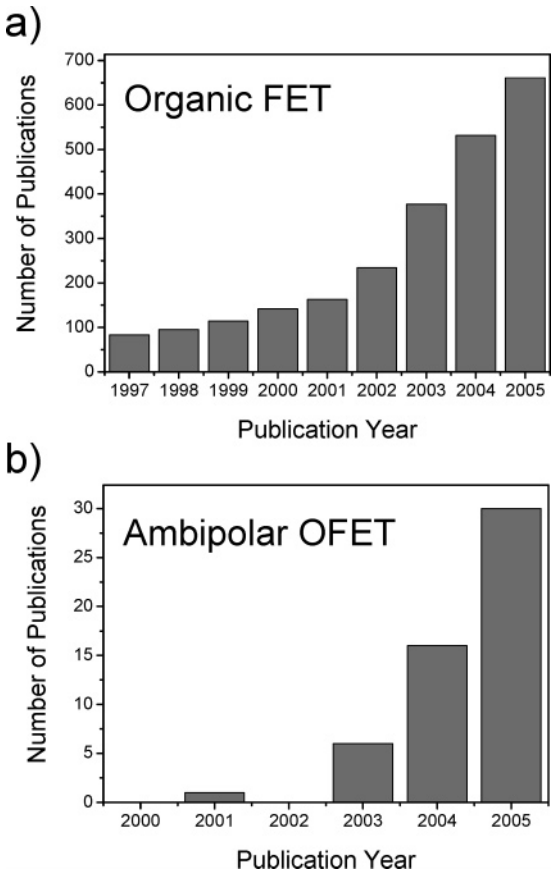

Figure 1. Number of publications on organic and polymer field-effect transistors **(a)** and ambipolar organic transistors **(b)** published over the past few years as counted by the Institute for Scientific Information (ISI) Web of Science.

In recent years it has become clear that the chemical structure of the organic semiconductor is not the only factor that determines whether an organic FET exhibits predominantly p-channel or n-channel behavior. Processing and characterization conditions, device architecture, and choice of electrodes are important as well. It is thus not appropriate to speak of p-type or n-type materials, but one should rather refer to p-channel or n-channel transistors. A key discovery was the identification of the crucial role of the gate dielectric and the identification of electron trapping mechanisms in devices based on SiO_2 gate dielectrics. This subsequently led to the general observation of n-channel and ambipolar characteristics in a broad range of polymer semiconductor FETs based on trap-free gate dielectrics.[21] This and other recent experimental and theoretical studies reviewed below suggest that organic semiconductors are intrinsically ambipolar and thus capable of conducting both electrons and holes in suitable device configurations and under inert testing conditions.

Here, we will give an overview on the working principles of organic field-effect transistors and describe how both hole and electron transport take place in these devices, which can be used to fabricate ambipolar and light-emitting transistors. Light-emitting transistors make use of the efficient radiative recombination of holes and electrons in organic semiconductors that leads to light emission from the transistor channel under certain biasing conditions and provides a direct visualization of ambipolar transport characteristics.

After introducing the basics of field-effect transistors and defining the parameters affecting their performance in

general, we will show what are the prerequisites for fabricating n-channel transistors and how those depend on processing conditions and device structure. Then we will introduce ambipolar field-effect transistors, which have only recently received increased attention (see Figure 1b), and their particular characteristics. Finally, both unipolar and ambipolar light-emitting transistors will be discussed.

2. Basics of Organic Field-Effect Transistors

Here we will introduce the basic structures and working principles of organic field-effect transistors, their current voltage characteristics, and how to extract information from them. We will briefly introduce the most common charge transport models and the role of the gate dielectric and injecting electrodes in organic FETs. Before moving on to n-channel transistors, we will briefly survey recently developed promising new materials for p-channel transistors.

2.1. Working Principle of FETs

A field-effect transistor (organic or inorganic) requires the following components (shown in Figure 2a): a thin semiconducting layer, which is separated from a gate electrode by the insulating gate dielectric; source and drain electrodes of width W (channel width) separated by a distance L (channel length) that are in contact with the semiconducting layer. The semiconducting layer in the case of an organic FET is usually vacuum sublimed, spin-coated, or drop-cast depending on the semiconductor. The gate electrode can be a metal or a conducting polymer, but very often, highly doped silicon serves as substrate and gate electrode at once. As

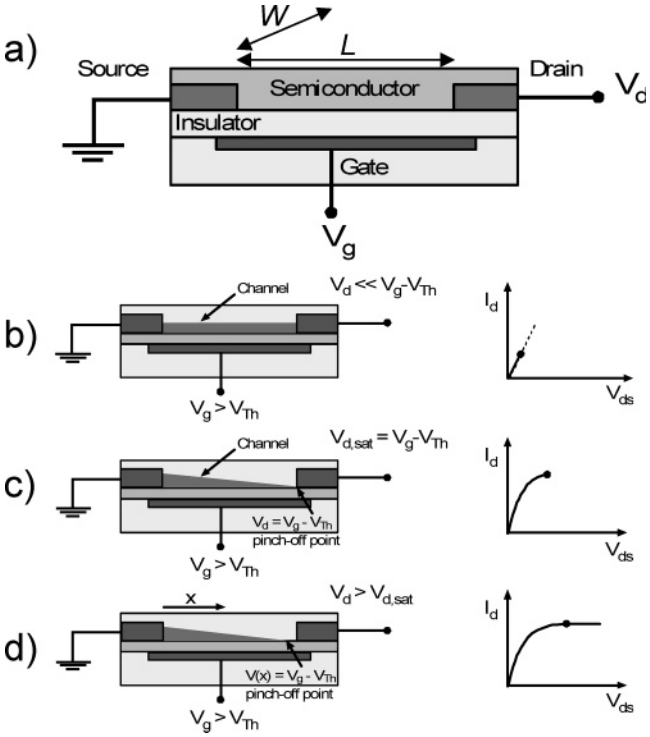

Figure 2. (a) Schematic structure of a field-effect transistor and applied voltages: L = channel length; W = channel width; V_d = drain voltage; V_g = gate voltage; V_{Th} = threshold voltage; I_d = drain current. (b−d) Illustrations of operating regimes of field-effect transistors: **(**b**)** linear regime; **(**c**)** start of saturation regime at pinch-off; **(**d**)** saturation regime and corresponding current−voltage characteristics.

gate dielectrics, inorganic insulators, such as, for example, SiO_2 (thermally grown on Si or sputtered), Al_2O_3, and Si_3N_4, or polymeric insulators, such as, for example, poly(methyl methacrylate) (PMMA) or poly(4-vinylphenol) (PVP)[22−24] are commonly used depending on the transistor structure. The source and drain electrodes, which inject charges into the semiconductor, are usually high work function metals such as gold (also Pd[25], Pt[26], and Ag[27,28]), but conducting polymers (e.g., PEDOT:PSS[29−31], PANI[32−34]), which can be printed, are used as well.

Voltage is usually applied to the gate electrode (V_g) and the drain electrode (V_d). The source electrode is normally grounded ($V_s = 0$). The potential difference between the source and the gate is usually just called the gate voltage (V_g), while the potential difference between the source and the drain is referred to as the source−drain voltage (V_{ds}). The source is the charge-injecting electrode, as it is always more negative than the gate electrode when a positive gate voltage is applied (electrons are injected) and more positive than the gate electrode when a negative gate voltage is applied (holes are injected).

Figure 2b−d illustrates the basic operating regimes and associated current−voltage characteristics of a field-effect transistor. First we can assume a simple metal−insulator−semiconductor (MIS) diode (that is, there is no potential difference between source and drain) with a voltage V_g applied to the gate electrode. A positive gate voltage for example will induce negative charges (electrons) at the insulator/semiconductor interface that were injected from the grounded electrodes. For negative V_g, positive charges (holes) will be accumulated. The number of accumulated charges is proportional to V_g and the capacitance C_i of the insulator. However, not all induced charges are mobile and will thus contribute to the current in a field-effect transistor. Deep traps first have to be filled before the additionally induced charges can be mobile. That is, a gate voltage has to be applied that is higher than a threshold voltage V_{Th}, and thus, the effective gate voltage is $V_g - V_{Th}$. On the other hand, donor (for n-channel) or acceptor (for p-channel) states and interface dipoles can create an internal potential at the interface and thus cause accumulation of charges in the channel when $V_g = 0$ so that in some cases an opposite voltage has to be applied to turn the channel off.[35,36]

When no source−drain bias is applied, the charge carrier concentration in the transistor channel is uniform. A linear gradient of charge density from the carrier injecting source to the extracting drain forms when a small source−drain voltage is applied ($V_{ds} \ll V_g$, Figure 2b). This is the linear regime, in which the current flowing through the channel is directly proportional to V_{ds}. The potential $V(x)$ within the channel increases linearly from the source ($x = 0$, $V(x) = 0$) to V_{ds} at the drain electrode ($x = L$, $V(x) = V_{ds}$).

When the source−drain voltage is further increased, a point $V_{ds} = V_g - V_{Th}$ is reached, at which the channel is "pinched off" (Figure 2c). That means a depletion region forms next to the drain because the difference between the local potential $V(x)$ and the gate voltage is now below the threshold voltage. A space−charge-limited saturation current $I_{ds,sat}$ can flow across this narrow depletion zone as carriers are swept from the pinch-off point to the drain by the comparatively high electric field in the depletion region. Further increasing the source−drain voltage will not substantially increase the current but leads to an expansion of the depletion region and thus a slight shortening of the

channel. Since the potential at the pinch-off point remains $V_g - V_{Th}$ and thus the potential drop between that point and the source electrode stays approximately the same, the current saturates at a level $I_{ds,sat}$ (Figure 2d).

Note that transistors with short channel lengths require thin gate dielectrics, typically $L > 10d_{dielectric}$,[37,38] in order to ensure that the field created by the gate voltage determines the charge distribution within the channel (gradual channel approximation) and is not dominated by the lateral field due to the source−drain voltage. Otherwise, a space−charge-limited bulk current will prevent saturation and the gate voltage will not determine the "on" or "off" state of the transistor.[39−44]

2.2. Current–Voltage Characteristics

The current−voltage characteristics in the different operating regimes of field-effect transistors can be described analytically assuming the gradual channel approximation. That is, the field perpendicular to the current flow generated by the gate voltage is much larger than the electric field parallel to the current flow created by the drain voltage. This is valid for long channel transistors but starts to fail for very short channel lengths; see above.

At a given gate potential higher than the threshold voltage V_{Th}, the induced mobile charges Q_{mob} per unit area at the source contact are related to V_g via

$$Q_{mob} = C_i(V_g - V_{Th}) \tag{2.1}$$

where C_i is the capacitance per unit area of the gate dielectric. In eq 2.1 the channel potential is assumed to be zero. However, the induced charge density depends on the position along the channel (x), which is accounted for in the following equation:

$$Q_{mob} = C_i(V_g - V_{Th} - V(x)) \tag{2.2}$$

Neglecting diffusion, the source−drain current (I_d) induced by carriers is

$$I_d = W\mu Q_{mob}E_x \tag{2.3}$$

where W is the channel width, μ is the charge mobility, and E_x is the electric field at x. By substituting $E_x = dV/dx$ and eq 2.2 into eq 2.3, we find

$$I_d\,dx = W\mu C_i(V_g - V_{Th} - V(x))\,dV \tag{2.4}$$

The gradual channel expression for the drain current can then be obtained by integration of the current increment from $x = 0$ to L, that is from $V(x) = 0$ to V_{ds}, assuming that the mobility is independent of the carrier density and hence the gate voltage:

$$I_d = \frac{W}{L}\mu C_i\left[(V_g - V_{Th})V_d - \frac{1}{2}V_{ds}^2\right] \tag{2.5}$$

In the linear regime with $V_{ds} \ll V_g$, this can be simplified to

$$I_d = \frac{W}{L}\mu_{lin}C_i(V_g - V_{Th})V_{ds} \tag{2.6}$$

The drain current is directly proportional to V_g, and the field-effect mobility in the linear regime (μ_{lin}) can thus be extracted from the gradient of I_d versus V_g at constant V_{ds} (also applicable for gate voltage dependent mobilities).

$$\mu_{lin} = \frac{\partial I_{ds}}{\partial V_g}\cdot\frac{L}{WC_iV_{ds}} \tag{2.7}$$

As described above, the channel is pinched off when $V_{ds} = V_g - V_{Th}$. The current cannot increase substantially anymore and saturates ($I_{ds,sat}$). Thus, eq 2.5 is no longer valid. Neglecting channel shortening due to the depletion region at the drain, the saturation current can be obtained by substituting V_{ds} with $V_g - V_{Th}$, yielding

$$I_{ds,sat} = \frac{W}{2L}\mu_{sat}C_i(V_g - V_{Th})^2 \tag{2.8}$$

In the saturation regime, the square root of the saturation current is directly proportional to the gate voltage. This equation assumes that the mobility is gate voltage independent. If this is not the case, a gate voltage dependent saturation mobility (μ_{sat}) can be extracted using

$$\mu_{sat}(V_g) = \frac{\partial I_{ds,sat}}{\partial V_g}\cdot\frac{L}{WC_i}\cdot\frac{1}{(V_g - V_{Th})} \tag{2.9}$$

Figure 3a shows typical output characteristics (that is the drain current versus source−drain voltage for different constant gate voltages) of a polymer n-channel transistor with a channel length of 200 μm. From the output characteristics, the linear regime at low V_{ds} and the saturation regime at high V_{ds} are evident.

Figure 3b shows the transfer characteristics (that is the drain current versus gate voltage at constant V_{ds}) of the same transistor in the linear regime ($V_{ds} \ll V_g$) both as a semilog plot and as a linear plot. From the semilog plot one can easily extract the onset voltage (V_{on}) (the voltage at which the drain current abruptly increases above a defined low off-current level) and the subthreshold swing ($S = dV_g/d(\log I_{ds})$), which depend on the gate dielectric capacitance and the trap states at the interface. The gradient of the current increase in the linear regime is directly proportional to the mobility according to eq 2.7 and is constant if the mobility is gate voltage independent. Most semiconductors, however, show gate voltage dependent mobilities, and thus, the curve shape may deviate from being linear.

Figure 3c shows a transfer curve in the saturation regime. Here the square root of the drain current should be linearly dependent on the gate voltage, and its gradient is proportional to the mobility according to eq 2.8. Extrapolating the linear fit to zero yields the threshold voltage V_{Th}.

Threshold voltages can originate from several effects and depend strongly on the semiconductor and dielectric used. Built-in dipoles, impurities, interface states, and, in particular, charge traps contribute to the threshold voltage.[23] Note that, independent of the cause of V_{Th}, it can be reduced by increasing the gate capacitance and thus inducing more charges at lower applied voltages. The threshold voltage is not necessarily constant for a given device. When organic transistors are operated for an extended time, V_{Th} tends to increase. This bias stress behavior has a significant effect on the applicability of organic transistors in circuits and is presently under intense investigation.[45−50] A shift of the threshold voltage on the time scale of current−voltage measurements causes current hysteresis (usually the forward scan shows higher currents than the reverse scan). Large,

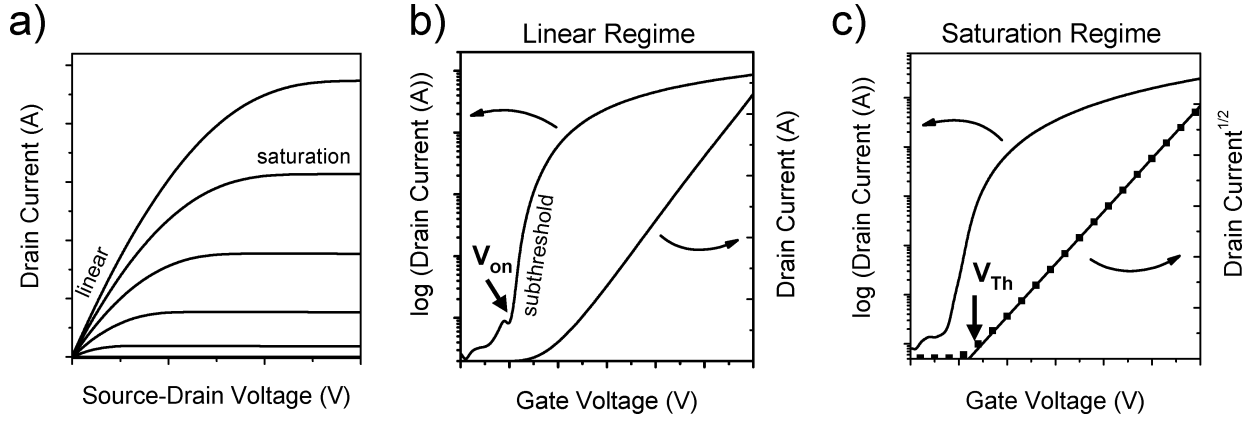

Figure 3. Representative current−voltage characteristics of an n-channel organic field-effect transistor: **(a)** output characteristics indicating the linear and saturation regimes; **(b)** transfer characteristics in the linear regime ($V_d \ll V_g$), indicating the onset voltage (V_{on}) when the drain current increases abruptly; **(c)** transfer characteristics in the saturation regime ($V_{ds} > V_g - V_{Th}$), indicating the threshold voltage V_{Th}, where the linear fit to the square root of the drain current intersects with the *x*-axis.

stable threshold shifts, e.g., induced by polarization of a ferroelectric gate dielectric, can be used in organic memory devices.[51,52]

Another important parameter of FETs that can be extracted from the transfer characteristics is the on/off ratio, which is the ratio of the drain current in the on-state at a particular gate voltage and the drain current in the off-state (I_{on}/I_{off}). For clean switching behavior of the transistor, this value should be as large as possible. In situations where contact resistance effects at the source−drain electrodes can be neglected, the on-current mainly depends on the mobility of the semiconductor and the capacitance of the gate dielectric. The magnitude of the off-current is determined by gate leakage, especially for unpatterned gate electrodes and semiconductor layers, by the conduction pathways at the substrate interface, and by the bulk conductivity of the semiconductor, which can increase due to unintentional doping, as for example often observed in P3HT transistors.[53−55]

2.3. Device Structures

The physical nature of the semiconductor as well as the employed gate dielectric may require or enable different device structures that can show very different transistor behavior. The most commonly found structures (in relation to the substrate) are the bottom contact/top gate (BC/TG, Figure 4a), bottom contact/bottom gate (BC/BG, Figure 4b), and top contact/bottom gate (TC/BG, Figure 4c) structures. Transistors with the same components but different geometries can show very dissimilar behavior.

One of the major differences between these device geometries arises from the position of the injecting electrodes in relation to the gate. In the bottom contact/bottom gate structure, charges are directly injected into the channel of accumulated charges at the semiconductor−dielectric interface. In the other two structures, the source/drain electrodes and the channel are separated by the semiconducting layer. Thus, charges first have to travel through several tens of nanometers of undoped semiconductor before they reach the channel. However, in the staggered BC/TG and TC/BG configurations, charges are injected not only from the edge of the electrode but also from those parts of the electrode that overlap with the gate electrode, contributing to the current depending on distance from the edge (current crowding).[56−58]

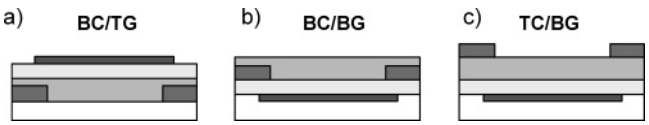

Figure 4. Common field-effect transistor configurations: **(a)** bottom contact, top gate (BC/TG); **(b)** bottom contact, bottom gate (BC/BG); **(c)** top contact, bottom gate (TC/BG).

Other differences between transistor structures arise from the dielectric/semiconductor and electrode/semiconductor interfaces, such as different morphologies at the top and bottom surfaces of a semiconductor film (molecular orientation, roughness)[59] or introduction of trap states during metal evaporation on organic semiconductors for top contact transistors.[60,61]

2.4. Charge Transport Models

The exact nature of charge transport in organic semiconductors is still open to debate. Nevertheless, one can make a clear distinction between disordered semiconductors such as amorphous polymers and highly ordered organic single crystals, at the opposite ends of the spectrum. Charge transport in disordered semiconductors is generally described by thermally activated hopping of charges through a distribution of localized states or shallow traps. Bässler et al. have described this density of states as a Gaussian distribution in order to model charge transport in time-of-flight experiments. The width of the Gaussian density of states is determined by the spatial and energetic disorder within the semiconductor and can be determined by temperature-dependent mobility measurements.[62] A broader density of states leads to lower mobilities and a stronger temperature dependence.

A variable range hopping model, where charges can hop a short distance with a high activation energy or a long distance with a low activation energy, was used by Vissenberg and Matters.[63] They further assumed an exponential distribution of localized states, which represents the tail of a Gaussian density of states, that dominates the transport characteristics at low carrier concentrations. The Vissenberg−Matters model predicts an increase of the field-effect mobility with increasing gate voltage, as the accumulated charge carriers fill the lower-lying states of the organic semiconductor first and any additional charges in the accumulation layer will occupy states at relatively high energies. Thus, additional charges will require a lower

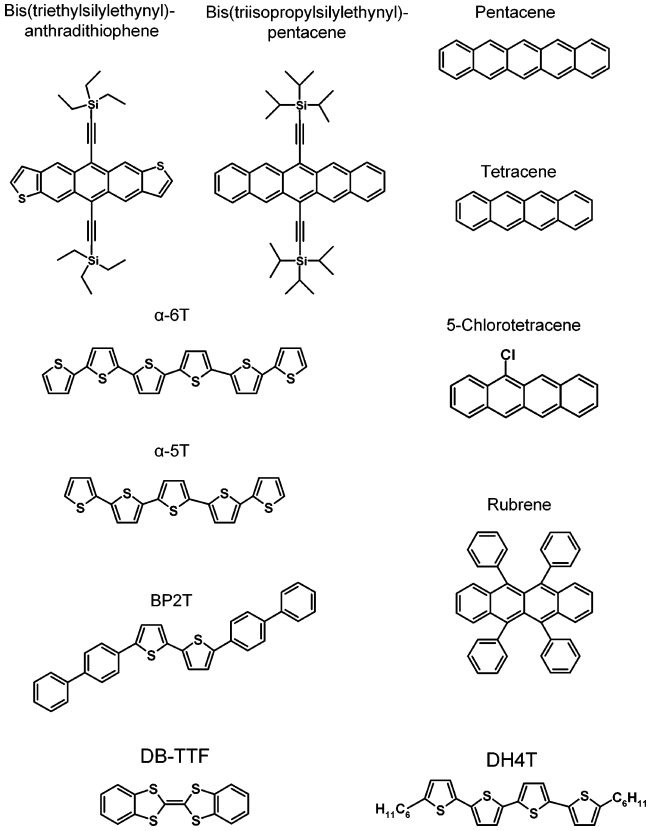

Figure 5. Small molecule semiconductors mentioned in the text, which are commonly known for their hole channel characteristics in field-effect transistors.

activation energy to hop between sites. This dependence of the mobility on charge density and thus gate voltage has been observed for many disordered semiconductors, and the Vissenberg−Matters model proved to be very useful to model organic field-effect transistors and reconcile charge mobilities in organic diode structures and field-effect transistors.[64−66]

For highly ordered molecular crystals such as, e.g., rubrene, tetracene, and pentacene (Figure 5), however, experimental data seems to exclude hopping transport. Temperature-dependent time-of-flight[67] and time-resolved terahertz pulse spectroscopy,[68,69] as well as recent field-effect transistor[70,71] measurements on high purity crystals showing high mobilities that increase with decreasing temperature, suggest bandlike transport in delocalized states instead of hopping transport. But at the same time, the mean free path of charge carriers at high temperatures (above 150 K) is found to be comparable with the crystal unit cell lattice parameters, which contradicts delocalized transport.[72,73] Recent theoretical studies suggest that thermal motion modulates the intermolecular electronic coupling (transfer integrals) between molecules in organic crystals due to their weak interaction, which could lead to localization of charge carriers even in highly ordered systems.[74,75] Furthermore, the polarizability of the gate dielectric can cause localization in organic single-crystal field-effect transistors, as shown by Hulea et al.[76]

Models for charge transport in organic semiconductors, such as polycrystalline thin films of small molecules and microcrystalline polymers that lie in between these two extreme cases, have been proposed as well.[77−79] Note that in all cases the transfer integral representing the electronic coupling of adjacent molecules and the polaronic relaxation energy, which is the energy gained when a charge geometrically relaxes over a single molecule or polymer segment, is an important parameter determining the probability of charge transport from one molecule to another and depends strongly on the particular molecule and the relative position of the interacting units. They are expected to be similar, although not necessarily the same, for holes and electrons.[80,81]

2.5. Role of Injecting Electrodes

Before a current can flow through the transistor channel, charges have to be injected from the source electrode into the semiconductor: that means, for n-channel transistors, injection of electrons into the LUMO level and, for p-channel transistors, injection of holes into the HOMO level of the semiconductor. Contrary to the case of silicon transistors, the contacts in organic field-effect transistors rely, with few exceptions,[82−84] on a direct metal−semiconductor junction without any doping. Thus, the metal−semiconductor interface is usually treated as a Mott−Schottky barrier, where the barrier height is given by the difference between the metal work function (φ) and the semiconductor HOMO or LUMO level. A good ohmic contact is expected when the work function of the injecting metal is close to the HOMO or LUMO level of the semiconductor.[85] Otherwise, a potential barrier is formed, leading to poor charge injection and non-ohmic contacts. This introduces an extra resistance to the transistor (contact resistance). Contact resistance can be measured as the voltage drop at the electrodes with non-contact scanning probe potentiometry (e.g., Kelvin probe),[86] by four-point probe measurements[87] or by determining the resistance of transistors with different channel lengths and extrapolating to zero channel length (transfer line method).[88,89] Depending on the mobility of the semiconductor, the channel length and gate voltage contact resistance can be significant or even larger than the channel resistance and thus dominate device performance.[57,90,91] This impacts, in particular, the linear regime of field-effect transistors because a large part of the source−drain voltage already drops at the contacts and not across the channel. High non-ohmic contact resistance typically manifests itself in the output characteristic of a transistor as an initially suppressed and then superlinear current increase in the linear region.

Comparing the work function of the injecting metal with the HOMO/LUMO levels of a semiconductor can help to determine whether charge injection is likely and whether high or low contact resistance is to be expected. For example, Bürgi et al. demonstrated that the work function of gold (φ = 5.1 eV) is well aligned with the HOMO level of P3HT (4.8 eV), which leads to a very low contact resistance, while for copper (φ = 4.7 eV) the contact resistance was several orders of magnitude higher and almost no charge injection from aluminum (φ = 4.0 eV) was observed.[86] However, the simple Mott−Schottky model is not always sufficient to describe contacts. Often, the interface exhibits an additional dipole barrier that tends to change the metal work function[92,93] and hence the interface barrier height. Intentionally introduced dipoles at the metal surface, e.g., through self-assembled monolayers, are useful to improve charge injection into organic semiconductors, as demonstrated by de Boer et al.[94] and Hamadani et al.[95]

Although the simple Mott−Schottky model provides a guideline for choosing appropriate injecting electrodes, it is

not sufficient to properly describe charge injection into organic semiconductors. Proposed models for that include thermally assisted tunneling from the metal to localized states,[96] tunneling into polaron levels,[97] thermally assisted injection into an energetically disordered dielectric,[98] or diffusion-limited thermionic emission.[99]

Additionally, contact resistance is not simply determined by the metal and the semiconductor but also by the device structure, e.g., whether a top contact or bottom contact geometry is employed. As mentioned above, the position of the injecting electrodes with respect to the gate electrode plays a role. In a staggered geometry (BC/TG and TC/BG) where the source and drain electrode overlap with the gate electrode, charges are injected over a larger area than in a coplanar (BC/BG) geometry. This current crowding leads to a lower contact resistance for the same material system.[56] Furthermore, while bottom contacts can be modified to alter their work function, evaporated metals may introduce surface states in the semiconductor that help or hamper charge injection.[60] More detailed descriptions of charge injection into organic semiconductors and organic metal interfaces were given in reviews by Shen et al.[100] and Kahn et al.[101]

2.6. Role of the Gate Dielectric

Comprehensive reviews about gate dielectrics for organic transistors were recently published by Facchetti et al.[24] and Veres et al.[23] Here we will only briefly introduce some of the main issues concerning dielectrics that will be important to understand their impact on hole and electron transport in FETs.

The crucial process of charge accumulation and transport in field-effect transistors takes place at and very close to the interface between the gate dielectric and the semiconductor; hence, the properties of this interface and the dielectric have a huge influence on device characteristics. Device parameters such as mobility, threshold voltage, subthreshold swing, etc. depend not only on the nature of the semiconductor but also on the chemical structure and dielectric properties of the insulator.

The requirements for gate dielectrics in field-effect transistors are rigorous. They should show high dielectric breakdown strength, contain only minimal concentrations of impurities that could act as traps, and be environmentally stable, easily processable, and compatible with preceding and subsequent processing steps. Apart from their breakdown strength, gate dielectrics are mainly characterized by their dielectric constant ε (also named k), which determines the capacitance $C_i = \varepsilon\varepsilon_0/d$ of a dielectric layer of thickness d (ε_0 is the permittivity in vacuum) and thus the amount of induced charges per applied V_g. Hence, in order to achieve a certain amount of charges in the transistor channel, one can either reduce the dielectric thickness or use a dielectric with a higher ε. The present dielectric of choice for studying and testing organic semiconductors is thermally grown silicon dioxide with a dielectric constant of $\varepsilon = 3.9$. The reason for this is the ready availability of doped silicon wafers with high quality, smooth, thermal SiO_2 that can also be used as substrates and give reproducible results for many semiconductors. Many groups investigated the influence of surface treatments of SiO_2 (e.g., with hexamethyldisilazane (HMDS) or self-assembled monolayers of different silanes) on the performance of organic transistors, looking at the change of morphology of semiconductor film, number of trap states, and dipoles at the surface.[35,102−105] Other metal oxides with higher ε such as, e.g., Al_2O_3 ($\varepsilon = 10$)[106,107] and Ta_2O_5 ($\varepsilon = 25$)[27,108] have also been investigated as possible gate dielectrics for organic transistors. Nevertheless, for the application of organic semiconductors in flexible electronics, SiO_2 and other oxides are not ideal dielectrics. In order to use them on flexible substrates, they usually need to be sputtered or anodized, which leads to inferior device performance.

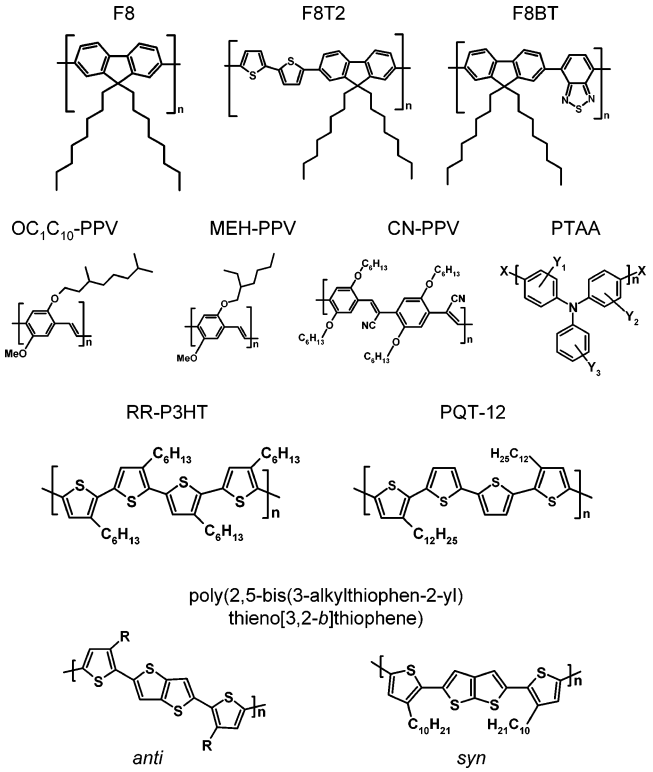

Figure 6. Conjugated semiconducting polymers mentioned in the text that have shown hole and, in some cases, electron field-effect transport: F8 (poly(9,9-dioctylfluorene)); F8T2 (poly(9,9-dioctylfluorene-alt-bithiophene)); F8BT (poly(9,9-dioctylfluorene-alt-benzothiadiazole)); OC_1C_{10}-PPV (poly(2-methoxy-5-(3,7-dimethyloctoxy)-*p*-phenylenevinylene)); MEH-PPV (poly(2-methoxy-5-(2-ethylhexoxy)-1,4-phenylenevinylene)); CN-PPV (poly(2,5-dihexoxy-α,α′-dicyano-*p*-xylylidene-alt-2,5-dihexoxy-*p*-xylylidene)); PTAA (poly(triarylamine)); RR-P3HT (regioregular poly(3-hexylthiophene)); PQT-12 (poly(3,3‴-didodecylquaterthiophene)); *syn*- and *anti*-poly(2,5-bis(3-alkylthiophen-2-yl)thieno[3,2-*b*]thiophene).

Another option are insulating polymers that can be processed from solution, that do not require high temperature processing, and whose characteristics can be tuned over a wide range by changing their chemical structure. Polymer gate dielectrics have been used in top as well as bottom gate transistors, and their impact on morphology and mobility was investigated.[109−114] They are easily applied in top gate transistors, where they are spun on top of the semiconductor from solvents orthogonal to the semiconductor and do not influence the interface morphology or damage the semiconductor.[30,37,115]

Veres et al. have recently shown that the influence of the gate dielectric is indeed more fundamental than just changing morphologies or the amount of induced charges. They found a direct dependence of the mobility of amorphous conjugated polymers based on triarylamines such as PTAA (Figure 6) and others on the dielectric constant of the employed gate dielectric.[23,115] They explained this observation with additional energetic disorder at the interface induced by dipolar

disorder in the dielectric, which increases with increasing ε. In the mobility model for disordered semiconductors by Bässler et al., an increase of energetic disorder leads to a broadening of the Gaussian density of states, which lowers the effective mobility.[62] A similar effect can be found in single-crystal rubrene transistors. But since transport in rubrene is not limited by disorder in the crystal, the lowered mobilities are likely to be due to disturbed delocalization.[76,116]

As shown above, the characteristics of organic FETs rely not only on the nature of the organic semiconductor but also on the nature of their injecting electrodes and gate dielectrics. This should be taken into account when comparing different FETs and their device characteristics.

2.7. Recent Developments for p-Channel FETs

The development of new materials for p-channel transistors continues to be a major area of research. Apart from high mobilities, major objectives are stability under ambient conditions and under bias stress, as well as easy processing, e.g., from solution, which would make organic semiconductors a viable alternative to amorphous silicon. For small molecule, thin-film transistors, pentacene (Figure 5) is still the material with the highest mobility, but it must be vacuum sublimed, while solution processing is technologically more practical. Various solution processable precursor forms of pentacene were synthesized and tested in field-effect transistors,[117,118] but they usually did not show as high mobilities as vacuum-sublimed films. Recently, new soluble pentacene derivatives with triisoalkylsilylethynyl groups at the 6,13-positions (Figure 5) were reported that show hole mobilities of up to 0.17 $cm^2\ V^{-1}\ s^{-1}$.[119,120] Similarly functionalized anthradithiophenes (triethylsilylethynyl anthradithiophene, Figure 5) showed even higher mobilities of up to 1 $cm^2\ V^{-1}\ s^{-1}$, probably due to improved π-stacking.[120−122]

Solution processable polymer semiconductors for p-channel transistors have also shown improved mobility and stability under ambient conditions in recent years. One of the most promising building blocks for polymer semiconductors remains thiophene. Regioregular poly(3-hexyl thiophene) (P3HT, Figure 6) used to be the conjugated polymer with the highest hole mobilities of up to 0.1 $cm^2\ V^{-1}\ s^{-1}$ depending on processing conditions.[103,123,124] P3HT, however, is very susceptible to unintentional doping due to its relatively low ionization potential (4.8 eV) and thus shows poor performance under ambient conditions. In order to increase the ionization potential while maintaining good transport properties, the conjugation length and thus delocalization of charges should be reduced. This can be achieved, e.g., by attaching alkyl chains only to some thienylene moieties and thus allowing more rotational freedom, which reduces the conjugation length. Ong et al. demonstrated this concept for poly(3,3‴-dialkylquaterthiophene)s (PQT-12, Figure 6), which exhibit high field-effect mobilities and good air stability.[125] An alternative approach is to incorporate a fused aromatic heterocycle that cannot form an extended conjugated pathway with both its neighboring monomer units, as shown for thieno[2,3-*b*]thiophene with sulfur atoms in *syn* position by Heeney et al.[126] Recently, the same approach using thieno[2,3-*b*]thiophene with sulfur atoms in *anti* position (Figure 6) yielded a liquid crystalline, reasonably air-stable semiconducting polymer that forms large crystals after annealing and shows the highest hole mobilities demonstrated for a semiconducting polymer up to now (0.6 $cm^2\ V^{-1}\ s^{-1}$).[127]

The highest mobilities and most intrinsic charge transport properties in organic semiconductors are, nevertheless, observed in single crystals. In recent years, single-crystal field-effect transistors were studied extensively, and a comprehensive review was given recently by de Boer et al.[128] Organic single crystals can be obtained through sublimation along a temperature gradient[129,130] (e.g., pentacene,[131] tetracene,[132] rubrene[133]) or grown in solution (e.g., tetrathiafulvalenes such as DB-TTF[134−136] or substituted acenes such as 5-chlorotetracene;[137] for chemical structures, see Figure 5). Due to the absence of spatial disorder and grain boundaries together with the low concentration of impurities and thus trap states, organic single crystals are ideal to study intrinsic charge transport in organic semiconductors and compare it with theoretical models.[75,138] High mobilities of up to 20 $cm^2\ V^{-1}\ s^{-1}$ in rubrene,[139] observation of the Hall effect,[71,140] and increasing mobility with decreasing temperature[70] are indicative of these properties and suggest bandlike charge transport. Organic single crystals can also show mobility anisotropy along different crystal axes,[141,142] which depends on molecular packing and thus different transfer integrals between neighboring molecules. Changing the crystal packing of semiconducting core molecules thus affects the field-effect mobility. This direct structure−property relationship in single crystals allows conceiving design rules for the development of new high mobility semiconductors.[120,122,135,143,144]

3. Organic n-Channel FETs

3.1. Motivation

For the development of electronic circuits based on organic semiconductors, logic elements are needed that go beyond single transistors. The most basic element is the voltage inverter, which inverts the incoming signal V_{in} into the outgoing signal V_{out}. Inverters are the basic circuit elements for logical functions such as NAND, NOR, and NOT. They are also used in ring oscillators, which consist of a series of inverters with the output of each inverter stage connected to the input of the following stage. The output of the last stage is then connected to the input of the first one. They are useful to demonstrate basic parameters of organic transistors given by their oscillation frequency and propagation delay per stage.

In silicon-based technology, inverters are complementary, consisting of a p- and an n-channel transistor where the gates are connected and serve as an input node (V_{in}). The drains of the two transistors are also connected and serve as an output node (V_{out}). The source of the driver transistor (usually the faster n-channel transistor) is grounded, and the source of the load transistor (usually the slower p-channel transistor) is connected to a power supply (V_{supply}). The circuit configuration of such a complementary inverter and an inverter transfer curve are shown in Figure 7. An important characteristic of a complementary inverter is that when the output is in a steady logic state ($V_{out} = 0$ or V_{supply}), only one transistor is "on" and the other one is in the "off" state. This reduces the current flow to a minimum of the leakage current through the transistors. Only during switching are both transistors on for a very short time. This considerably reduces power consumption compared to other circuit architectures.

Although it is possible to fabricate inverters with only one type of transistors (e.g., p-channel), as demonstrated with organic transistors based on various materials,[145−151] it is

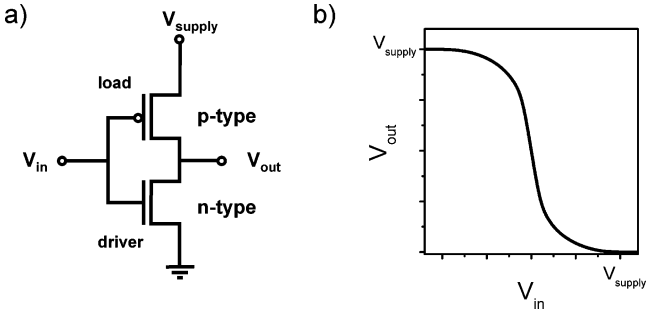

Figure 7. (a) Schematic circuit configuration of a complementary inverter based on a p-channel and an n-channel transistor. (b) Transfer curve of a complementary voltage inverter.

advantageous to use complementary circuit design for organic logic as well. Apart from the low static power dissipation, complementary circuits show more robust operation, show better noise margins, and are easier to design. In order to achieve organic complementary inverters, it is necessary to fabricate reliable organic n-channel transistors that can be integrated with p-channel transistors. The vast majority of organic transistors in the literature are p-channel transistors. However, in recent years, the need to build complementary circuits has fueled research into n-channel and also ambipolar transistors, which led to an increase of n-channel transistors being demonstrated over the past few years as well as organic complementary inverters and more complex circuits.[152−160]

Apart from these technological reasons, it is important to investigate electron transport in organic semiconductors from a fundamental scientific point of view. Although most of the nowadays available organic semiconductors seem to preferentially show p-channel behavior, there is no obvious reason why these materials should not also exhibit n-channel behavior. Although reorganization energies and transfer integrals of holes and electrons are not necessarily the same, theoretical studies show that they are at least similar for many organic semiconductors (polymers and small molecules). Electrons are thus not inherently much less mobile than holes in most organic semiconductors.[80,81] Hence, it is essential to find out what are the intrinsic or extrinsic reasons for the rare observation of n-channel behavior in organic FETs.

In the following, we will give a short overview of the problems and challenges that fabricating n-channel organic transistors entails and how these can be overcome by rational synthetic approaches. A more detailed treatise of these issues was recently given by Newman et al.,[161] and the reader is referred to this review for more details. Here we will focus on the intrinsic capability of known organic semiconductors to conduct electrons as well as holes depending on the device structure, processing and testing conditions.

3.2. Problems and Challenges

One of the main challenges of fabricating a n-channel transistor is the injection of electrons into the LUMO level of the semiconductor from a suitable electrode. For p-channel transistors, the injection of holes into the HOMO level is easily achieved using gold electrodes because the HOMO level of many organic semiconductors is in the range of 4.8 to 5.3 eV, which aligns well with the work function of gold (4.8−5.1 eV). The LUMO level, on the other hand, often lies much higher, at around 2−3 eV. When gold electrodes are used in this case, observation of n-channel behavior cannot be expected due to the extremely high injection barrier of 2−3 eV. In order to inject electrons, one needs to use low work function metals, such as calcium, magnesium, or aluminum, that are not environmentally stable. Most newly synthesized organic semiconductors are tested using convenient gold electrodes, and thus n-channel transport may not be observed due to the misalignment of the LUMO level with the work function of gold.

Another major obstacle is the susceptibility of organic semiconductors to water and oxygen under ambient conditions. Organic radical anions as they are present in the channel when a positive gate voltage is applied have a very high reducing power and can thus react with water or oxygen that have diffused into the organic film.[162] Many n-channel transistors can thus only operate when processed and tested under inert conditions excluding oxygen and water, which makes them technologically unattractive.

3.3. Design Rules and New Materials

In order to fabricate n-channel transistors that can be processed under the same conditions and with the same electrodes as those used for p-channel transistors, many new materials were synthesized. A number of design rules have guided the search for these so-called "n-type" semiconductors. In order to be able to inject electrons into the LUMO level from environmentally stable electrodes, such as gold, the LUMO level must be lowered (i.e., increasing the electron affinity) substantially in order to align with the work function of the metal. At the same time, increasing the electron affinity of a semiconducting material also improves its environmental stability, that is, its sensitivity to oxygen and water. On the basis of known n-channel transistors, it was generally assumed that a high electron affinity (at least 3 eV) is necessary to observe n-channel behavior.[161] This is achieved by taking a known semiconducting core molecule and adding strong electron withdrawing groups such as fluorine, cyano, or diimide moieties. At the same time, the molecular packing of those molecules might be altered due to these changes, which could impede or improve electron transfer. A class of molecules with exceptionally high electron affinity are the fullerenes and their derivatives (e.g., C_{60} and PCBM, Figure 8). They were shown to yield n-channel transistors with very high electron mobilities.[163−165] Although a high electron affinity improves the environmental stability of the organic semiconductor, the radical anion remains thermodynamically unstable, especially toward oxygen in the presence of water. A kinetic barrier against diffusion of water and air into the active channel region during operation is needed. Very close packing of molecules, as was shown for fluorinated copper phthalocyanine,[166] seems to be beneficial in that respect.

Very few of the demonstrated n-channel transistors are stable under ambient conditions; among them are transistors based on fluorinated copper phthalocyanine (FCuPC),[166] dicyanoperylene-3,4:9,10-bis(dicarboximide) (PDI-8CN_2),[153,167] and α,ω-diperfluorohexylsexithiophene (DHF-6T)[168] (chemical structures in Figure 8).

In addition to stability and energetic considerations, the orientation of molecules to each other and the associated transfer integrals of electrons play a role. The best LUMO−LUMO overlap for electron transport may be different from the ideal HOMO−HOMO overlap for hole transport.[80,81] Facchetti et al. showed that the molecular packing in crystalline semiconductors can strongly affect the observation of p- or n-channel characteristics.[169,170] This may be less important for amorphous polymer semiconductors. Neverthe-

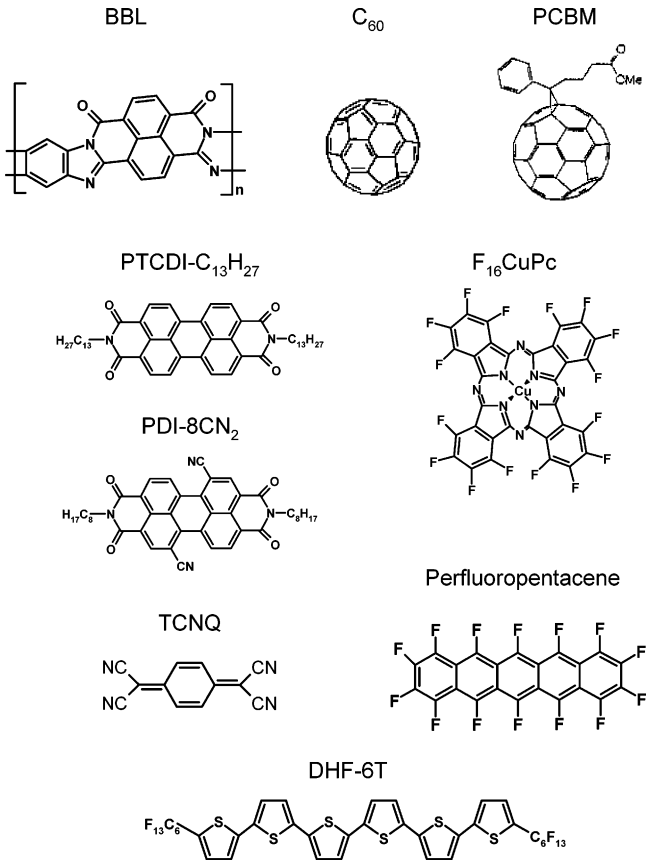

Figure 8. Organic semiconductors mentioned in the text that show predominantly n-channel behavior in transistors with SiO_2 as a gate dielectric and gold source−drain electrodes.

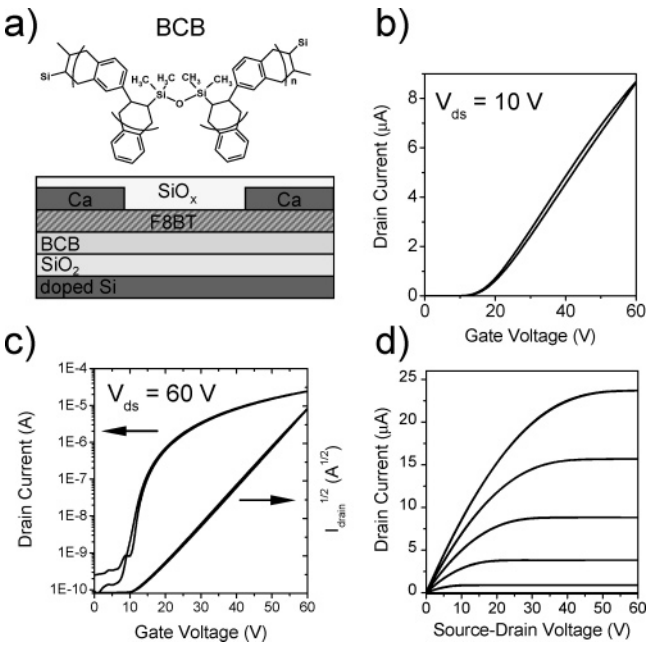

Figure 9. (a) Schematic illustration of an n-channel transistor fabricated on a doped silicon/thermal silicon dioxide substrate with BCB (inset) as a buffer dielectric, F8BT as a polymer semiconductor, evaporated calcium top electrodes, and a capping layer of silicon monoxide. Linear **(b)** and saturation regime **(c)** transfer characteristics of a transistor as shown in (a) with $L = 200$ μm and $W/L = 500$, indicating an almost gate voltage independent electron mobility of 4.5×10^{-3} cm^2 V^{-1} s^{-1} and a turn-on voltage of 11 V. **(d)** Output characteristics of the same transistor showing good saturation and nearly no contact resistance.

less, one of the few conjugated polymers showing n-channel behavior until recently was poly(benzobisimidazobenzophenanthroline) (BBL, Figure 8).[171]

3.4. Role of Dielectric for Electron Transport

Apart from the air-sensitivity of many materials, it remained puzzling why plenty of materials showed electron transport in time-of-flight measurements, light-emitting diodes (LEDs), and photovoltaic cells but when the same materials were used in transistor structures, even with low work function electrodes, no n-channel behavior was observed. One example is the conjugated polymer poly(9,9-di-*n*-octylfluorene-alt-benzothiadiazole) (F8BT, Figure 6). Due to the electron withdrawing properties of the benzothiadiazole (BT) group, F8BT exhibits a relatively high electron affinity (EA) of 3.3 eV and a large ionization potential (IP) of 5.9 eV. It is often used as an electron transporter in polymer blend LEDs[172−174] and photovoltaic cells.[175−177] F8BT should thus be a good candidate for electron transport in field-effect transistors as well. However, no n-channel behavior is observed in F8BT transistors that use SiO_2 as a gate dielectric and calcium top contact electrodes. On the other hand, when a buffer layer of an apolar polymer dielectric is introduced to a device structure, n-channel characteristics appear immediately.[21] Figure 9a shows the device structure for such an n-channel transistor. A crosslinked benzocyclobutene derivative (BCB, inset Figure 9a) serves as the buffer dielectric between silicon dioxide and the semiconductor. The obtained transfer and output curves show near ideal n-channel current−voltage characteristics (Figure 9b−d). Very little hysteresis is observed in continuous forward and reverse voltage sweeps, the electron mobility (5×10^{-3} cm^2 V^{-1} s^{-1}) is nearly gate voltage independent, and the output characteristics show good saturation and essentially no contact resistance. This striking difference between the behavior observed at the F8BT/BCB interface and that observed at the F8BT/SiO_2 interface can be explained by the chemical nature of the dielectric/semiconductor interface. While the cured BCB contains essentially no hydroxyl groups, native SiO_2 as it is used for standard testing of transistors has a large number of OH-groups (silanol groups) at the surface that are able to trap electrons irreversibly. When electrons are trapped at the dielectric/semiconductor interface, they induce an electric field opposed to the applied gate voltage, thus shifting the threshold for electron accumulation well outside the usually accessible range.

This assumption can be tested by fabricating F8BT transistors with different buffer dielectrics without OH-groups such as polyethylene (PE) and poly(*p*-xylylene) (Parylene N), which also enable n-channel behavior, and with OH-containing buffer dielectrics such as poly(4-vinylphenol) (PVP), with which no electron transport is observed.

Another way of passivating the silanol groups on the SiO_2 surface is the treatment with HMDS or self-assembled monolayers (SAMs) of alkylsilanes (Figure 10a). And indeed, electron transport is observed for F8BT transistors with self-assembled monolayers of octadecylsilane, decylsilane, and butylsilane on the SiO_2 dielectric. But during operation, for example, during a transfer scan with $V_{ds} = 60$ V and $V_{g,max} = 60$ V, irreversible trapping takes place and the threshold shifts rapidly to higher voltages. All devices cease working after a certain time of continuous stress due to this threshold shift. The threshold voltage shift and the rate of electron

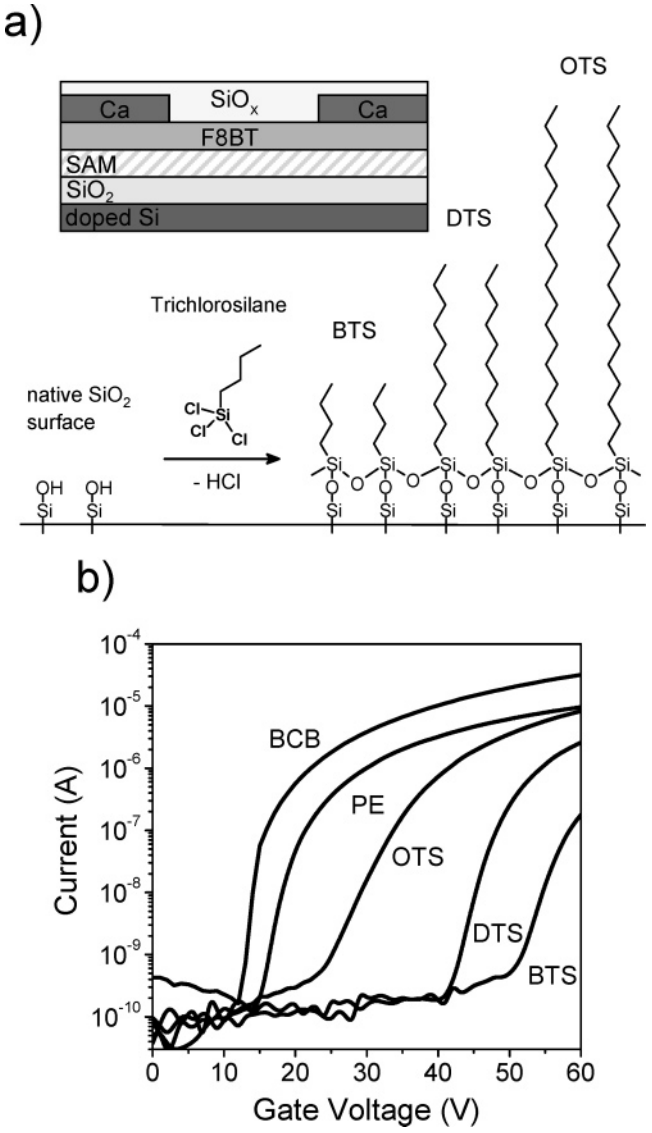

Figure 10. (a) Schematic illustration of a F8BT transistor with self-assembled monolayers of alkylsilanes on the SiO_2 surface. The different alkylsilane monolayers are assembled by the reaction of octadecyl-, decyl-, and butyltrichlorosilane (OTS, DTS, and BTS) with the hydroxyl groups on the SiO_2 surface. **(**b**)** Second forward transfer scan at $V_{ds} = 60$ V of F8BT transistors with BCB or polyethylene (PE) as buffer dielectrics and with self-assembled alkylsilane monolayers on the SiO_2 dielectric. The increasing thresholds indicate the amount of trapped electrons at the dielectric/semiconductor interface.

trapping correlate with the length of the alkyl chains. This is demonstrated in Figure 10b, where the second forward scans for F8BT transistors with BCB and polyethylene as buffer dielectrics and those with self-assembled monolayers (SAMs) of alkylsilanes are shown. Shorter alkyl chains lead to larger threshold shifts than longer chains. But for all SAMs, the threshold voltages shift up to the maximum applied gate voltage after prolonged operation. This clearly suggests that alkyl SAMs do not passivate all silanol groups at the interface and merely act as a tunneling barrier for electrons before those can reach the remaining OH-groups at the surface.

Knowing that BCB buffer layers enable electron transport in F8BT transistors, representatives of various families of conjugated polymers were tested, among them those that are known for their good hole mobilities and some with electron

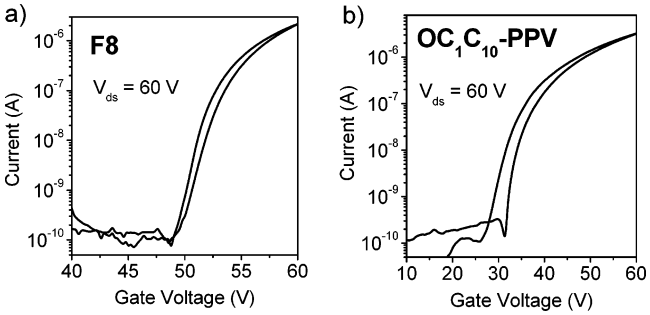

Figure 11. Transfer characteristics of n-channel FETs with the same device structure as in Figure 9a using **(a)** poly(9,9-dioctylfluorene) (F8) and **(**b**)** poly(2-methoxy-5-(3,7-dimethyloctoxy)-*p*-phenylenevinylene) (OC_1C_{10}-PPV) as the semiconducting layer.

affinities as low as 2.6 eV. The polyfluorenes F8 (Figure 11a) and F8T2, the poly(phenylenevinylene)s (PPVs) CN-PPV, MEH-PPV, and OC_1C_{10}-PPV (Figure 11b), and the polythiophene P3HT (chemical structures in Figure 6) all showed clear n-channel behavior with BCB as a buffer dielectric and evaporated calcium top electrodes. Their electron mobilities were of similar magnitude to those measured for holes.[21]

Similar effects were shown for CN-poly(dihexylfluorene-vinylene)[178] and, more interestingly, for pentacene[179] on poly-(chloro-*p*-xylylene), also using calcium electrodes. On the other hand, Singh et al. demonstrated n-channel transport in pentacene on poly(vinyl alcohol) (PVA) as a gate dielectric while the same device configuration with poly(4-vinylphenol) (PVP) did not show any electron transport.[180] Both dielectrics contain large numbers of hydroxyl groups, although with different acidities.

Benson et al. demonstrated n-channel behavior of pentacene with poly(methyl methacrylate) (PMMA) as a dielectric and calcium electrodes and mobilities of about 0.1 $cm^2\ V^{-1}\ s^{-1}$. UV treatment of the PMMA in air and thus formation of hydroxyl, hydroperoxide, carbonyl, and carboxyl groups prevented observation of electron transport and instead enabled p-channel behavior.[181]

Note that the impact of electron traps such as hydroxyl groups at the semiconductor/insulator interface is highest for materials with low electron affinities. Organic semiconductors with very high electron affinities, such as, for example, PCBM (EA = 3.7 eV) and FCuPc (EA = 4.8 eV), show good n-channel behavior on SiO_2 dielectrics. Yoon et al. found that the electron mobility in organic semiconductors with high electron affinity (EA > 4 eV) was less affected by surface treatment and the presence of electron traps than lower electron affinity materials.[182]

In conclusion, the observation of electron transport in many organic semiconductors previously only considered to be capable of hole transport shows that electron transport is not a property limited to a specific class of high electron affinity materials, but is actually a generic feature of many undoped organic semiconductors. In addition to the injecting electrodes, the gate dielectric must be chosen carefully in order to avoid trapping of electrons and thus enable observation of the intrinsic n-channel behavior.

4. Ambipolar Field-Effect Transistors

4.1. Motivation

As mentioned in section 3, the complementary approach to fabricating integrated circuits is superior to the unipolar

approach, showing low power dissipation, wide noise margins, and higher robustness.[154] Unlike in silicon-based technology, where p- and n-channel transistors are created by implantation of dopants on a submicrometer scale, laterally controlled deposition of two different organic materials on a substrate requires a number of additional process steps, increasing the process complexity and thus the manufacturing cost significantly. Hence, ambipolar device architectures or materials that can provide both n- and p-channel performance and thus enable complementary-like inverters without advanced patterning techniques are desirable. Another advantage of ambipolar inverters is that they work for both positive and negative V_{in} and V_{out}, depending on the supply voltage V_{supply}, unlike unipolar inverters, which only work for one polarity. However, in such an ambipolar inverter, neither transistor is ever fully switched off, and thus, leakage currents increase power dissipation and lower the switching speed compared to those of complementary inverters with unipolar n- and p-channel transistors.

From a scientific perspective, the ability to realize ambipolar transistors, which accumulate and conduct both holes and electrons, enables new ways to improve the understanding of the physics of these organic devices. In particular, direct comparison of hole and electron transport within the same device and the recombination of opposite charge carriers within the transistor channel that can result in light emission are intriguing subjects.

As we will see below, a series of paths have been followed to achieve ambipolar behavior in organic field-effect transistors. Here we divide them into three major groups with respect to the semiconducting layer: bilayer, blend, and single-component transistors. They all have particular characteristics and advantages. But first we will introduce the common working principles and device characteristics of ambipolar transistors and the particular challenges that arise from them. In order to view organic ambipolar transistors in the context of other technologies, we will also briefly introduce two other material systems that show ambipolar transport: amorphous silicon and carbon nanotubes. Amorphous silicon is in many ways comparable to organic semiconductors, and many concepts of amorphous silicon FETs have been applied to organic FETs. Carbon nanotubes were the first carbon-based materials for which ambipolar transport and associated light emission were reported.

4.2. Device Characteristics and Challenges of Ambipolar FETs

An ambipolar transistor is one in which both electrons and holes are accumulated depending on the applied voltages. They exhibit characteristic transfer and output curves, which can be understood easily, considering the potentials applied to the source, drain, and gate electrodes relative to one another.

Let us assume a transistor at a given positive drain voltage V_d (the source potential is held at ground, $V_s = 0$) and start with a positive gate voltage of $V_g = V_d$. Just as in a unipolar transistor, the gate is more positive than the source electrode and thus electrons are injected from the source into the accumulation layer and drift toward the drain, given that $V_g > V_{Th,e}$ ($V_{Th,e}$ = threshold for electron accumulation). Only one polarity of charge carriers is present, and we call this the unipolar regime. When, on the other hand, V_g is smaller than V_d, the gate potential is more negative than that of the drain electrode by $V_g - V_d$. While, for $V_g < V_{Th,e}$, the source will not inject electrons, the drain electrode in an ambipolar transistor will inject holes into the channel if $V_g - V_d < V_{Th,h}$ ($V_{Th,h}$ = threshold for hole accumulation). Thus, one should actually now speak of the drain electrode as a hole source. A hole current will flow, and thus, the measured drain current will be high, not like in a unipolar, n-channel transistor, which would now be in an off-state. If the gate potential is somewhere between V_d and V_s so that it is bigger than $V_{Th,e}$ but also $V_g - V_d < V_{Th,h}$ (Figure 12a), both the source and drain electrode will inject the respective charge carriers and thus both electrons and holes are present in the channel. This regime is called the ambipolar regime, in contrast to the unipolar regime, where only one polarity of charges is present in the channel for any particular biasing condition.

In an ideal ambipolar transistor with just one semiconducting layer, the ambipolar regime is characterized by a hole and an electron accumulation layer next to the respective electrode that meet at some point within the transistor channel (inset of Figure 12b). There, oppositely charged carriers recombine. In electroluminescent materials, this leads to light emission from within the channel, which will be discussed in section 5. The length of each channel and thus the meeting point and position of the recombination zone depend on the applied gate and source−drain voltage and mobility ratio. The potential of the transistor channel in the ambipolar regime can roughly be imagined as that of a saturated hole and electron channel in series, resulting in an s-shaped transition region (Figure 12b), as theoretical studies show.[183−185]

The transfer curves of ambipolar transistors exhibit a characteristic V-shape with one arm indicating electron transport and the other indicating hole transport (see Figure 12c). For positive (negative) applied voltages, the effective gate voltage for holes (electrons) depends on the applied source−drain voltage, which gives rise to the characteristic dependence of the transfer characteristics on the source−drain voltage. The output curves are characterized by a superposition of standard saturated behavior for one carrier at high V_g and a superlinear current increase at low V_g and high V_{ds} due to injection of the opposite carrier (Figure 12d).

One of the challenges of fabricating ambipolar transistors lies in the efficient injection of both charge carriers. Optimal charge injection takes place when the work function of the metal electrode lines up with the HOMO level of the semiconductor for hole injection and with the LUMO level for electron injection. Since most of the standard organic semiconductors have band gaps of 2−3 eV, the injection of at least one carrier must be contact limited for any given electrode material. Another challenge is trapping of one or both carrier types. We have seen that especially electrons are likely to be trapped by impurities or certain chemical moieties at the dielectric/semiconductor interface. This can be prevented by using appropriate dielectrics, using pure materials, and processing in an inert atmosphere. The stability of hole and electron transport under ambient conditions, and thus exposure to moisture and oxygen, is another issue.

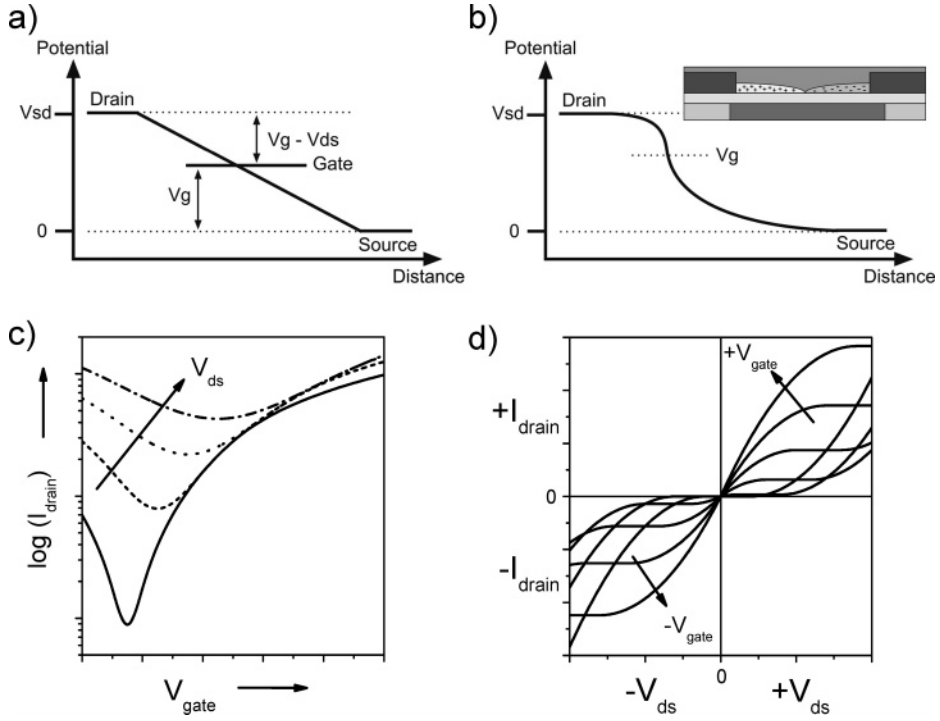

Figure 12. (a) Illustration of the source, drain, and gate potentials with respect to each other in a field-effect transistor. **(b)** Channel potential in a field-effect transistor in the ambipolar regime with two separate channels of holes and electrons that meet within the transistor channel, where opposite charge carriers recombine (inset). **(c)** Calculated transfer characteristics for an ambipolar transistor with equal hole and electron mobilities and slightly different threshold voltages in a semilog plot for positive gate voltages and different positive source−drain voltages. **(d)** Calculated ambipolar output characteristics for the same transistor for positive (first quadrant) and for negative (third quadrant) V_g and V_{ds}, respectively.

4.3. Amorphous Silicon and Carbon Nanotube Ambipolar FETs

Amorphous and polycrystalline silicon thin-film transistors are a key component of active matrix flat panel displays, switching individual pixels on and off. In particular, hydrogenated amorphous silicon (a-Si:H) is suitable for this application because it can be deposited over large areas. Thin-film transistors with a-Si:H usually work in electron accumulation mode. However, about three decades ago, Neudeck and Malhotra[186] found the first evidence for ambipolar transport in a-Si:H FETs using aluminum injecting electrodes. More detailed studies and modeling were carried out by Pfleiderer et al.[187,188] and Hack et al., who also proposed light-emitting transistors based on amorphous silicon.[189] But, since silicon has an indirect band gap and thus radiative recombination is very inefficient, no such silicon-based light-emitting transistor has yet been demonstrated. Amorphous silicon transistors show hole mobilities that are about two orders of magnitude lower than the electron mobilities (0.1−1 $cm^2\ V^{-1}\ s^{-1}$) due to specific defects in the vicinity of the valence band and thus were not interesting technologically.[190] Nevertheless, they proved useful to investigate bias stress behavior and trapping in a-Si:H transistors.[191,192]

Carbon nanotubes are quasi-one-dimensional objects with unique electronic properties and are attracting increasing attention due to their interesting physics and potential application in electronics and sensing. Depending on their internal chirality, they can show metallic or semiconducting behavior.[193] Field-effect transistors based on semiconducting single-walled carbon nanotubes (s-SWNTs)[194] can be tuned to be p-type, n-type, or ambipolar by using appropriate injecting electrodes or doping. Despite their small radius (1−2 nm), SWNTs can sustain large currents, due to the exceptionally high mobility (>1000 $cm^2\ V^{-1}\ s^{-1}$) of charge carriers. Five-stage ring oscillators based on p- and n-type transistors fabricated on the same SWNT reach frequencies of up to 52 MHz,[195] demonstrating potential for nanoelectronic applications. Vacuum-annealed SWNT-FETs with titanium electrodes show ambipolar characteristics due to thin Schottky barriers at the source and drain contacts that allow thermally assisted tunneling of holes and electrons into the nanotube and thus ambipolar transport.[196] When the gate is biased in between the source and the drain potential, polarized infrared light is emitted from the nanotube due to the radiative recombination of injected holes and electrons.[197] The wavelength of emission depends on the diameter and thus the direct band gap of the carbon nanotube. Freitag et al. showed that the location of recombination and emission is controlled by the gate voltage and can be resolved in long (100 μm) SWNT transistors. During a constant current scan, the emission zone moves with changing gate voltage from the drain to the source and vice versa.[198]

4.4. Organic Bilayer FETs

The idea to achieve ambipolar (sometimes also referred to as bipolar) behavior in organic field-effect transistors by using bilayers of n-channel and p-channel semiconducting materials (here meaning semiconductors with high and low electron affinity, respectively) in the same device was first proposed and demonstrated by Dodabalapur and co-workers more than a decade ago.[199,200] They combined layers of the known hole-conducting α-hexathienylene (α-6T, Figure 5) and the electron-conducting C_{60} (Figure 8) and observed both

hole and electron transport in these devices, although with lower mobilities than those for each material on its own. They pointed out that choosing the materials carefully according to the relative position of their HOMO and LUMO levels as well as the deposition order were important for achieving ambipolar characteristics. At the time, however, only a few p-channel materials and even less reliable n-channel materials were available, which may explain why this approach only recently has been revived by a number of groups. Rost et al. showed that a bilayer structure of pentacene and PTCDI-$C_{13}H_{27}$ (chemical structure in Figure 8) with a gold electrode for hole injection and a magnesium electrode for electron injection exhibits ambipolar current−voltage characteristics[201] with apparent electron and hole mobilities of 3×10^{-3} cm^2 V^{-1} s^{-1} and 1×10^{-4} cm^2 V^{-1} s^{-1}), respectively. Inoue et al. reported higher balanced mobilities of 0.04 cm^2 V^{-1} s^{-1} for a bilayer device using pentacene on top of perfluorinated pentacene (chemical structure Figure 8) on top of gold electrodes. Bilayers of pentacene and C_{60} have also been proven to exhibit ambipolar transport by several groups.[202,203] Dinelli et al. investigated bilayers of α,ω-dihexylquarterthiophene (DH4T, Figure 5) and PTCDI-$C_{13}H_{27}$ and found ambipolar behavior for both sequences of deposition.[204] While the electron mobility for both deposition sequences remained similar (0.03−0.04 cm^2 V^{-1} s^{-1}), the hole mobility varied by an order of magnitude (0.03 cm^2 V^{-1} s^{-1} for PTCDI-$C_{13}H_{27}$ on DH4T and 0.002 cm^2 V^{-1} s^{-1} for DH4T on PTCDI-$C_{13}H_{27}$), which was assigned to the inferior film forming properties of DH4T on PTCDI-$C_{13}H_{27}$. They also observed light emission in these devices, which will be discussed later.

Apart from these very different material combinations, one pair of organic semiconductors seems to be particularly well-suited to achieve ambipolar behavior as well as air stability: copper phthalocyanine (CuPc) and fluorinated copper phthalocyanine (FCuPc). These phthalocyanines are particularly suitable for sublimation deposition on top of each other, as they show similar molecular shapes and crystal structures. FCuPc is a well-known air-stable n-type semiconductor with very high electron affinity (4.8 eV) and ionization potential (6.3 eV) due to the electron withdrawing F atoms.[166] The mobility of electrons in FCuPc can be as high as 0.03 cm^2 V^{-1} s^{-1}. CuPc, on the other hand, shows good hole mobilities (0.04 cm^2 V^{-1} s^{-1}); it has a moderate electron affinity of 3.1 eV and an ionization potential of 5.0 eV. Ambipolar transistors based on bilayers of these materials were reported by several groups.[205−209] The highest ambipolar mobilities (3.3×10^{-3} cm^2 V^{-1} s^{-1} for both holes and electrons) for this combination were found by Ye et al. for a bilayer structure with CuPc on top of FCuPc that was grown at 120 °C on a SiO_2 dielectric.[207]

Air-stable, ambipolar transistors based on FCuPc as an efficient electron conductor and 2,5-bis(4-biphenylyl)-bithiophene (BP2T, Figure 5) as a hole conductor were reported by Wang et al.[210] Figure 13 shows the output and transfer characteristics of such a device. With this bilayer combination, ambipolar mobilities of up to 0.04 cm^2 V^{-1} s^{-1} for holes and 0.036 cm^2 V^{-1} s^{-1} for electrons are possible under ambient conditions. Inverters fabricated with these transistors showed high gains of 13 and good noise margins.

For all the above-mentioned devices, one can assume that charge accumulation and transport of holes and electrons occur in different layers of the device structure. For example, for the CuPc on FCuPc case, electrons are injected

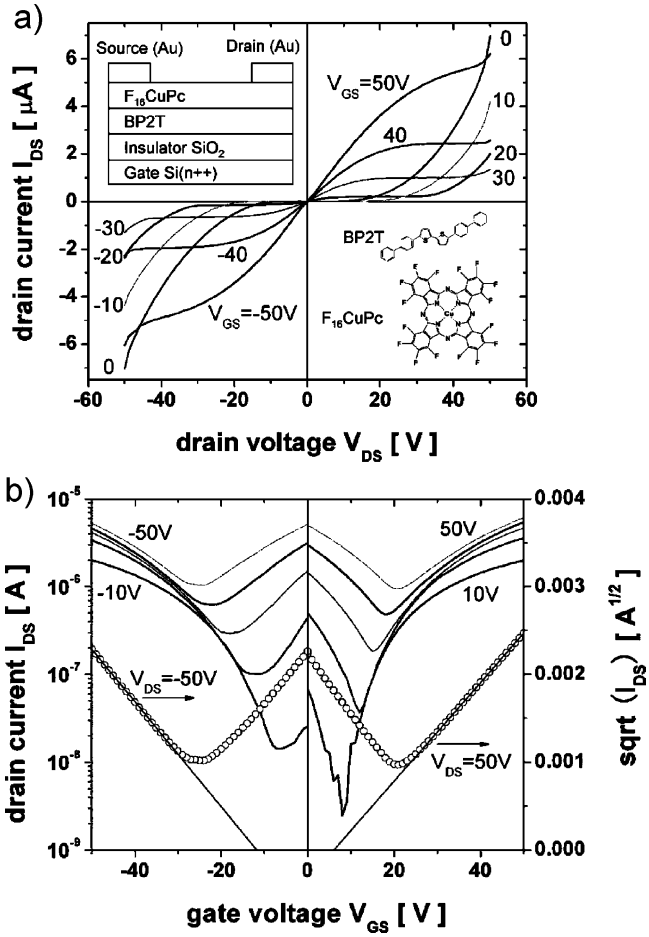

Figure 13. (a) Typical output characteristics of ambipolar OFETs based on FCuPc and BP2T bilayers for positive and negative gate biases. A schematic cross section of the device structure and the molecular structures of FCuPc and BP2T are given in the insets. **(**b**)** Typical transfer characteristics for positive and negative gate biases. The solid lines show the logarithmic drain current vs gate voltage for various V_{ds}, and the open symbols show the square root of the drain current. Reused with permission from Haibo Wang, Jun Wang, Zuanjun Yan, Jianwu Shi, Hongkun Tian, Yanhou Geng, and Donghang Yan, Applied Physics Letters, 88, 133508 (2006) (ref 210). Copyright 2006, American Institute of Physics.

from the gold electrodes into the CuPc and then into the FCuPc, due to its higher electron affinity. Charge transport then occurs at the FCuPc/SiO_2 interface. On the other hand, at negative gate voltages when holes are injected into the CuPc, they will remain there and do not cross into the FCuPc because that would be energetically unfavorable. The hole accumulation layer is thus formed at the CuPc/FCuPc interface and charge transport will depend on the quality of that interface.[205] For some material combinations, one has to expect intermixing and rough interfaces, which are known to impede charge transport. Hence, growth conditions play a role for improving ambipolar mobilities in bilayer devices.

All examples of bilayer ambipolar transistors use sublimed thin films. To the best of our knowledge, no ambipolar bilayer transistors based on solution-processed semiconductors, e.g., semiconducting polymers, have been demonstrated up to now. This seems mainly due to the problem of fabricating well-defined smooth bilayer structures by spinning one polymer on top of another, lamination, or spontaneous vertical phase separation.

4.5. Organic Blend FETs

Although the bilayer approach yields some impressive device characteristics and interesting insight into the electronic properties of organic semiconductor heterointerfaces, its main disadvantage remains the need to deposit two layers on top of each other. Furthermore, cheaper solution processable options for bilayers are challenging due to the need for finding an orthogonal solvent for the deposition of the second layer. An alternative method is to use blends of n- and p-channel materials and thus realize ambipolar transport in a single layer. For the blend approach, both coevaporated and solution-processed films are feasible.

The investigated material systems for coevaporated small molecule films overlap with those of the bilayer approach. Rost et al. showed that coevaporating PTCDI-$C_{13}H_{27}$ and α-quinquethiophene (α-5T, Figure 5) with equal fractions results in good ambipolar characteristics (Figure 14) with hole and electron mobilities of 1×10^{-4} cm^2 V^{-1} s^{-1} and 1×10^{-3} cm^2 V^{-1} s^{-1}, respectively, which were again smaller than those for the pure materials.[211] This can be understood in terms of interpenetrating networks of n-channel and p-channel materials, which predominantly conduct one or the other carrier due to their different electron affinities and ionization potentials, and thus, the effective mobilities of both electrons and holes in a percolating network are lower compared to that of a neat film. Loi et al. later investigated

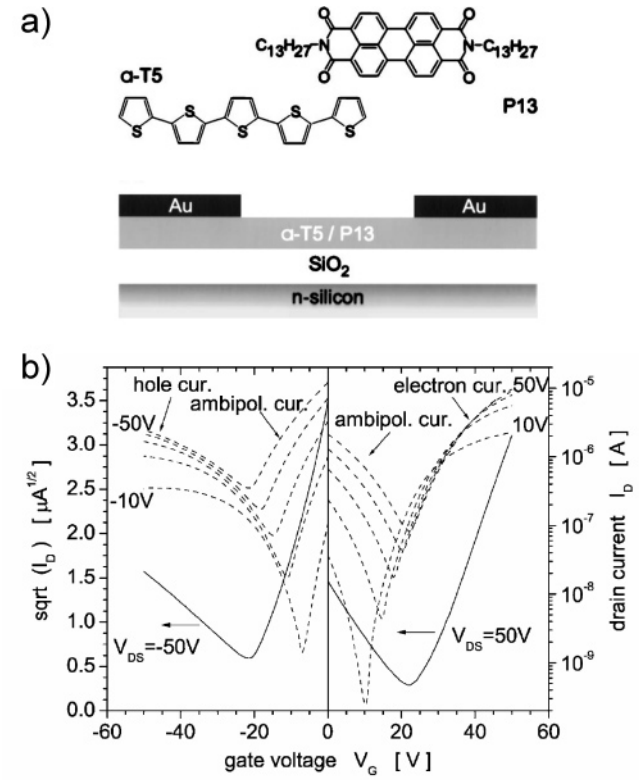

Figure 14. (a) Molecular structure of α-5T and PTCDI-$C_{13}H_{27}$ and device structure of an ambipolar field-effect transistor consisting of a coevaporated thin film of α-5T and PTCDI-$C_{13}H_{27}$. **(b)** Transfer characteristics of the coevaporated α-5T/PTCDI-$C_{13}H_{27}$ thin-film transistor for negative and positive gate biases. The solid lines show the square root of the drain current, and the dashed lines show the logarithmic drain current versus gate voltage for various source−drain voltages V_{ds}. Reused with permission from Constance Rost, Siegfried Karg, Walter Riess, Maria Antonietta Loi, Mauro Murgia, and Michele Muccini, Applied Physics Letters, 85, 1613 (2004) (ref 211). Copyright 2004, American Institute of Physics.

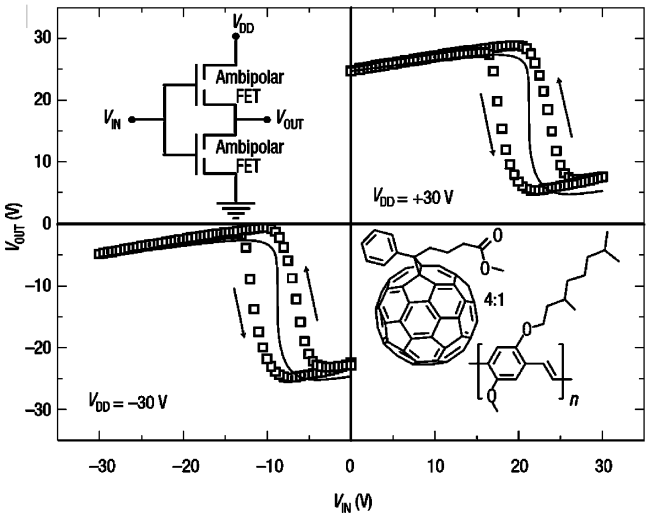

Figure 15. Transfer characteristics of complementary-like inverters based on two identical ambipolar OC_1C_{10}-PPV/PCBM field-effect transistors. Depending on the polarity of the supply voltage V_{DD}, the inverter works in the first or the third quadrant. A schematic representation of the inverter and the chemical structures of OC_1C_{10}-PPV and PCBM are given in the insets. Reprinted by permission from Macmillan Publishers Ltd: Nature Materials (ref 216), copyright 2003.

the impact of the relative fractions of each material on hole and electron mobilities in the same system[212] and found the expected increase of hole mobility with an increasing fraction of α-5T and equally an enhanced electron mobility with an increasing PTCDI-$C_{13}H_{27}$ fraction. Balanced hole and electron mobilities for this system are anticipated for a PTCDI-$C_{13}H_{27}$/α-5T ratio of 2:3. These blends also show light emission, which will be discussed in section 5. Other coevaporated systems resulting in ambipolar transport include pentacene/PTCDI-$C_{13}H_{27}$[213] and pentacene/fluorinated pentacene.[214]

Thin films of polymer blends are easily processable and thus well suited for application in integrated circuits. Their microstructure can be tuned by the choice of solvents and spin conditions.[177] The first ambipolar FETs based on a blend were fabricated by Tada et al. by mixing the electron conducting dye *N*,*N*′-bis(2,5-di-*tert*-butylphenyl)-3,4,9,10-perylene dicarboximide, whose chemical structure is similar to PTCDI-$C_{13}H_{27}$, with p-type poly(3-dodecylthiophene) in chloroform and spinning this mixture on a Si/SiO_2 substrate with prepatterned Ti/Au electrodes.[215] Although ambipolar behavior was observed, the effective mobilities were extremely low (10^{-7} cm^2 V^{-1} s^{-1} for holes and 10^{-9} cm^2 V^{-1} s^{-1} for electrons).

The first demonstration of a polymer blend transistor with appreciable ambipolar mobilities was accomplished by Meijer et al. by blending poly(2-methoxy-5-(3,7-dimethyloctoxy)-*p*-phenylene vinylene) (OC_1C_{10}-PPV, Figure 6) and [6,6]-phenyl C_{61}-butyric acid methyl ester (PCBM, Figure 8).[216] Here, the hole and electron mobilities reached 7×10^{-4} cm^2 V^{-1} s^{-1} and 3×10^{-5} cm^2 V^{-1} s^{-1}, respectively. Singh et al. found that the ambipolar characteristics of these blend films depend strongly on the nature of the dielectric they are spun upon and the resulting film morphology.[217] More recently, blends of poly(2-methoxy-5-(2′-ethylhexyloxy)-1,4-phenylenevinylene) (MEH-PPV) and C_{60},[218] MEH-PPV and PCBM,[52] CuPc and poly(benzobisimidazo-benzophenanthroline),[219] P3HT and PCBM,[220] as well as a thieno[2,3-*b*]-thiophene terthiophene polymer and PCBM[221] have shown

ambipolar transport with hole and electron mobilities in the 10^{-4} to 10^{-3} cm^2 V^{-1} s^{-1} range. Inverters fabricated with such blends (see Figure 15) show high gain[216,221] and thus could be suitable for integrated circuits.

4.6. Single-Component Ambipolar FETs

4.6.1. Fullerene Derivatives

Fullerenes and their derivatives have been known as n-type semiconductors for some time[163,164] and thus were applied in bilayer and blend ambipolar transistors. Recently, however, they were shown to have ambipolar characteristics as pure materials as well. Anthopoulos et al. showed that the well-known, solution processable n-channel material PCBM also exhibits p-channel characteristics with gold electrodes on HMDS-treated SiO_2 as the dielectric, despite the mismatch of the gold work function and both the HOMO and LUMO levels of PCBM.[222,223] The effective mobilities for electrons and holes were similar (1×10^{-2} and 8×10^{-3} cm^2 V^{-1} s^{-1}, respectively). Transistors fabricated with analogues to PCBM with C_{70} and C_{84} fullerenes instead of C_{60} also show ambipolar characteristics and are more reproducible and less air-sensitive than PCBM.[90,224] Other C_{60} derivatives with oligothiophene (Figure 16a)[225] and 9-(1,3-dithiol-2-ylidene)-thioxanthene (Figure 16b)[226] groups, that act as π-electron donors, attached to the fullerene exhibit both hole and electron accumulation, although with very low mobilities ($\sim 10^{-5}$ cm^2 V^{-1} s^{-1}).

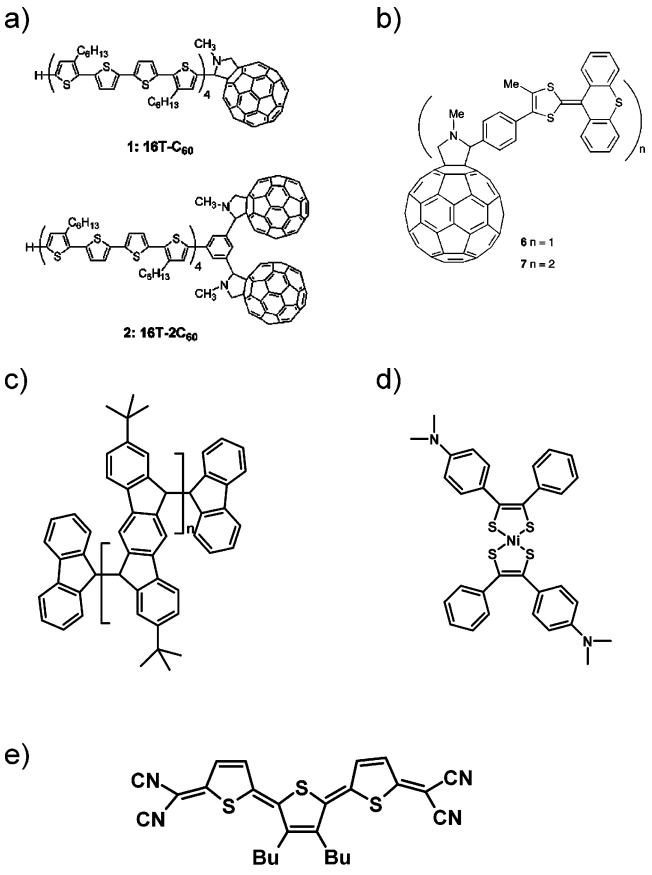

Figure 16. Selection of recently demonstrated materials showing ambipolar transport in field-effect transistors: **(a)** oligothiophene/fullerene dyad and oligothiophene/fullerene triad;[226] **(b)** 9-(1,3-dithiol-2-ylidene)thioxanthene-C_{60} system ($n = 6$);[225] **(c)** poly(3,9-di-*tert*-butylindeno[1,2-*b*]fluorene) (PIF);[216] **(d)** the near-infrared absorbing dye bis[4-dimethylaminodithiobenzyl]nickel (nickel dithiolene);[239] **(e)** quinoidal terthiophene (DCMT).[235]

4.6.2. Single Crystals

Organic single crystals are seen as model systems for charge transport in organic semiconductors, as they are free of grain boundaries, have a low concentration of trap states, and thus show very high field-effect mobilities. Hence, it is interesting to see whether intrinsic ambipolar transport is achievable in single-crystal field-effect transistors as well. Most single-crystal FETs, however, only show p-channel behavior.[128] Menard et al. demonstrated the first single-crystal n-channel FET based on tetracyanoquinodimethane (TCNQ, Figure 8), with electron mobilities of 1.6 cm^2 V^{-1} s^{-1}.[139] The benchmark molecule for single-crystal p-channel transistors is rubrene. Transistors based on rubrene crystals show high hole mobilities of up to 20 cm^2 V^{-1} s^{-1}.[70,139] Recently, rubrene single crystals also showed ambipolar transport, although only in vacuum and with an electron mobility of 0.01 cm^2 V^{-1} s^{-1}, which was more then 2 orders of magnitude smaller than the hole mobility in the same crystal.[227] In these devices, poly(methyl methacrylate) (PMMA) was used as the gate dielectric and silver electrodes were used instead of the usual gold electrodes, which facilitated electron injection due to their lower work function. But high contact resistance was still apparent and may be one cause of the low effective electron mobility. Sublimed thin films of rubrene also show ambipolar characteristics in vacuum, although with extremely low mobilities for both holes and electrons (10^{-6} cm^2 V^{-1} s^{-1}).[228]

Ambipolar transport in single crystals of copper phthalocyanine (CuPc) and iron phthalocyanine (FePc) was demonstrated by de Boer et al.[229] The hole mobilities for both materials reached 0.3 cm^2 V^{-1} s^{-1}; however, the electron mobilities were limited to 1×10^{-3} cm^2 V^{-1} s^{-1} in CuPc and 0.03 cm^2 V^{-1} s^{-1} in FePc. Note that thin films of CuPc also show ambipolar behavior when poly(chloro-*p*-xylylene) as a dielectric and Ca/Ag electrodes are employed.[230] Hole and electron mobilities of 2.5×10^{-4} cm^2 V^{-1} s^{-1} and 1×10^{-3} cm^2 V^{-1} s^{-1}, respectively, are observed in these thin-film devices. Since gold electrodes were used in the single-crystal CuPc and FePc FETs, high contact resistance for electron injection may have lowered the apparent electron mobility. Thus, information on intrinsic electron transport in these systems is very limited. Undoubtedly, more work needs to be done to reveal intrinsic ambipolar charge transport in organic single-crystal FETs.

4.6.3. Pentacene Thin Films

One of the most well-known and highest mobility p-channel organic semiconductors is pentacene. Field-effect mobilities in sublimed thin films and in single crystals reach up to 5 cm^2 V^{-1} s^{-1}.[25,114,131,231] But pentacene also shows n-channel behavior, which was first demonstrated by Meijer et al. with thin pentacene films on HMDS-treated SiO_2 and gold bottom contact source−drain electrodes.[216] However, electron mobilities were extremely low (10^{-6} cm^2 V^{-1} s^{-1}) and could only be observed in vacuum. Pentacene thin films on poly(chloro-*p*-xylylene) as the gate dielectric with calcium top electrodes showed somewhat better n-channel performance. These devices exhibited ambipolar behavior with hole and electron mobilities of 4.5×10^{-4} cm^2 V^{-1} s^{-1} and 2.7×10^{-5} cm^2 V^{-1} s^{-1}, respectively. The low hole mobility was assigned to the barrier for injection of holes from calcium into the HOMO level of pentacene.[179,232] Much higher mobilities were reported by Singh et al. for pentacene films on poly(vinyl alcohol) (PVA) as the gate dielectric and

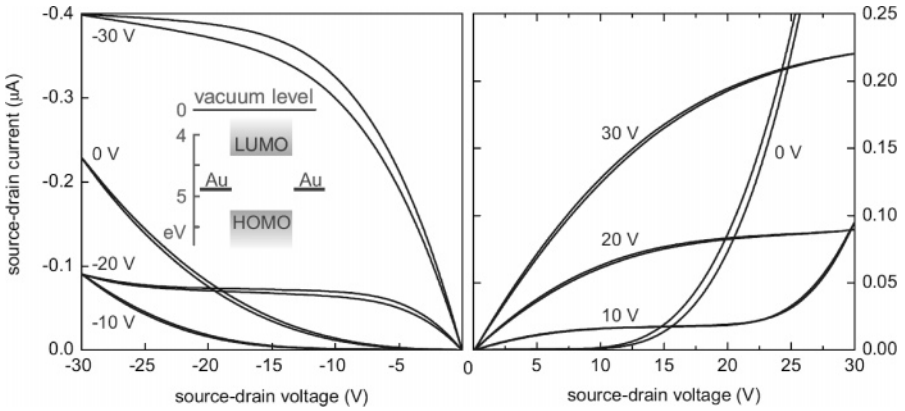

Figure 17. Output characteristics of a nickel dithiolene-based ambipolar transistor (channel length = 10 μm; channel width = 20 mm) with Ti/Au electrodes and HMDS-treated SiO_2 as a gate dielectric at room temperature. Transistor fabrication and characterization were performed under ambient conditions. Reprinted with permission from ref 239. Copyright 2006 Wiley-VCH Verlag GmbH & Co. KGaA.

with gold top electrodes for both hole and electron injection.[180,233] The maximum hole and electron mobilities in those devices were 0.5 and 0.2 $cm^2\ V^{-1}\ s^{-1}$, respectively. Schmechel et al. also achieved ambipolar transport in pentacene by doping the insulator/semiconductor interface with a sub-monolayer of Ca and using a calcium electrode for electron injection and a gold electrode for hole injection.[183]

4.6.4. Narrow Band Gap Semiconductors

As already mentioned, injection of both holes and electrons into a particular semiconductor is one major obstacle to overcome in order to fabricate ambipolar FETs. Most common organic semiconductors (small molecules and polymers) show band gaps between 2 and 3 eV. Thus, injection from a metal electrode with a given work function (high or low) will always result in high injection barriers (>1 eV) for either electrons or holes. Meijer et al. first pointed out that this dilemma could be solved by using semiconductors with a very narrow band gap[216] of less than 1.8 eV. Thus, the injection barrier for both charge carriers is lowered and efficient ambipolar transport can take place. This concept was successfully demonstrated by the same group with poly(3,9-di-*tert*-butylindeno[1,2-*b*]fluorene) (PIF, Figure 16c),[216] which has a band gap energy of 1.55 eV.[234] Using bottom contact gold electrodes and HMDS-treated SiO_2 substrates, the obtained hole and electron mobilities were 4×10^{-5} $cm^2\ V^{-1}\ s^{-1}$ and 5×10^{-5} $cm^2\ V^{-1}\ s^{-1}$, respectively. Other ambipolar transistors based on low band gap materials include DCMT (E_{gap} = 1.85 eV, Figure 16e),[235] the metallofullerene Dy@C_{82} (E_{gap} = 0.2 eV),[236] TiOPc (E_{gap} = 1.7 eV),[237] lead phthalocyanine PbPc (E_{gap} = 1.2 eV),[238] and a range of near-infrared absorbing dyes including bis-[4-dimethylaminodithiobenzyl]nickel (E_{gap} = 0.9 eV, Figure 16d).[239,240] The latter is solution processable and shows air-stable ambipolar transport with almost no contact resistance (see output characteristics in Figure 17). Electron and hole mobilities are in the range of 10^{-4} $cm^2\ V^{-1}\ s^{-1}$. An integrated five-stage ring oscillator fabricated with these transistors reached a maximum oscillation frequency of 710 Hz. Low band gap semiconductors are thus a very promising route for ambipolar transistors in flexible electronics.

4.6.5. High/Low Work Function Electrodes

Another way to avoid the problem of unequal charge carrier injection into a semiconductor is the use of source and drain electrodes with unequal work functions. We have already seen that many organic semiconductors that usually show p-type behavior with standard gold electrodes can also show n-type behavior with low work function electrodes such as calcium[21,241] or aluminum[242] and suitable trap-free gate dielectrics. Thus, using, e.g., a gold electrode for hole injection and a calcium electrode for electron injection in the same device should lead to ambipolar behavior even for wide band gap semiconductors. Schmechel et al. demonstrated this for ambipolar pentacene transistors where subsequent angled evaporation of calcium and gold as top contact electrodes led to the desired asymmetry of injecting electrodes.[183] Hole and electron mobilities in these devices were on the order of 0.1 $cm^2\ V^{-1}\ s^{-1}$.

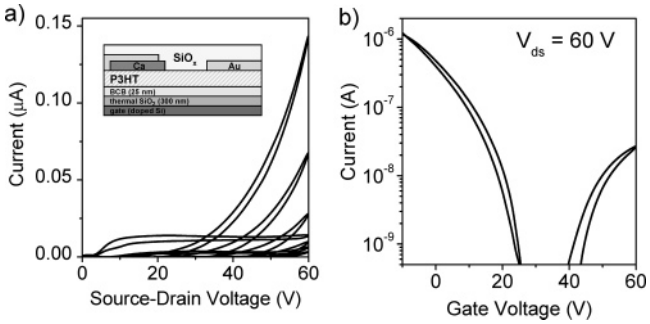

Figure 18. (a) Output (V_g from 0 to 60 V in steps of 10 V) and **(**b**)** transfer characteristics (V_{ds} = 60 V) of an ambipolar P3HT transistor with asymmetric evaporated calcium/gold top contact source−drain electrodes and BCB as a buffer dielectric. The schematic device structure is given in the inset to part a.

This approach of combining trap-free gate dielectrics with asymmetric contacts is also useful to show the ambipolar characteristics of one of the standard p-channel conjugated polymers: P3HT. Figure 18 shows the device structure, output, and transfer characteristics of such an ambipolar P3HT transistor with Ca/Au electrodes.[243] Due to the very low electron affinity of P3HT, the threshold for electron transport is very high despite the use of BCB as a hydroxyl-free dielectric. The apparent hole and electron mobilities of 6×10^{-3} $cm^2\ V^{-1}\ s^{-1}$ and 3×10^{-4} $cm^2\ V^{-1}\ s^{-1}$, respectively, in this device are fairly low, which is probably due to inferior microstructural order at the P3HT/BCB interface in comparison to the high order usually achieved for P3HT on HMDS-treated SiO_2, but are consistent with time-of-flight data that also shows ambipolar transport.[244]

On the basis of this concept, ambipolar charge transport was also found in poly(phenylenevinylene)s such as OC_1C_{10}-PPV and SuperYellow.[245,246] The use of trap-free gate dielectrics and asymmetric work function electrodes could enable ambipolar transport in an even wider range of materials and thus allow studying their intrinsic charge transport behavior and possibly resulting light emission.

4.6.6. Bottom Contact/Top Gate Ambipolar F8BT FETs

As we have seen, overcoming contact resistance is important for achieving ambipolar transport in organic transistors as well as using a suitable gate dielectric. For material systems with high contact resistance, an alternative approach is to select a device configuration in which contact resistance effects can be minimized. In a bottom contact/bottom gate (coplanar) structure, the injecting electrodes are in direct contact with the accumulation layer, but the injection area is limited to the side wall of the source−drain contacts. On the other hand, in a bottom contact/top gate (staggered) structure, charges are injected into the semiconductor from below the accumulation layer and, thus, have to cross an undoped semiconductor region before reaching the actual conducting channel. In this case charges are injected not only from the edge of the electrode but also from the surface of the contacts in the region where the source−drain electrodes overlap with the gate electrode. This leads to current crowding and becomes particularly important for devices with high injection barriers. Charges injected away from the edges of the contacts lead to an effective lengthening of the channel but also a reduction of contact resistance compared to the case of a device configuration in which injection is only possible at the edge of the source−drain electrodes. The contact resistance in staggered geometries is greatly reduced compared to that of the coplanar geometry, as was shown, e.g., for F8T2 transistors by Street et al.[56]

We found that the bottom contact/top gate structure can allow injection of holes and electrons from an electrode material such as gold into polymer semiconductors with relatively wide band gaps.[21] This is demonstrated in Figure 19 for ambipolar transistors with F8BT as the semiconductor, which has a band gap of 2.6 eV. These devices were fabricated on a glass substrate with photolithographically defined interdigitated gold electrodes, spun and annealed F8BT as the semiconductor, and spin-cast PMMA as a polymer gate dielectric on top. Evaporating gold as the gate electrode completed the transistor structure. Despite the high barriers for injection of both holes and electrons from gold into F8BT that are predicted to be on the order of 1−1.3 eV on the basis of a simple Mott−Schottky model, the transistors show efficient and stable ambipolar transport with balanced hole and electron mobilities of about 8×10^{-4} cm^2 V^{-1} s^{-1} (Figure 19).[247] As expected, a large contact resistance is evident in the output characteristics as a suppressed and then superlinear current increase at low V_{ds} (Figure 19). The threshold voltages for hole and electron transport in these devices are on the order of −20 and 30 V, respectively. Bottom contact/bottom gate transistors with F8BT and gold electrodes do not exhibit ambipolar transport. This shows that ambipolar transport in organic FETs depends on the particular device geometry just as well as on the employed materials. Exploiting this property could allow more varied material choices for ambipolar transistors in the future.

For completeness, we include here the synthetic approach of Yoon et al., who found ambipolar transport characteristics in thin-film transistors with certain carbonyl-functionalized quaterthiophenes (optical $E_{gap} = 2.6-2.8$ eV) using HMDS-treated SiO_2 as a dielectric and top gold electrodes.[248] These transistors showed good electron mobilities (as high as 0.6 cm^2 V^{-1} s^{-1}) and about two orders of magnitude lower hole mobilities.

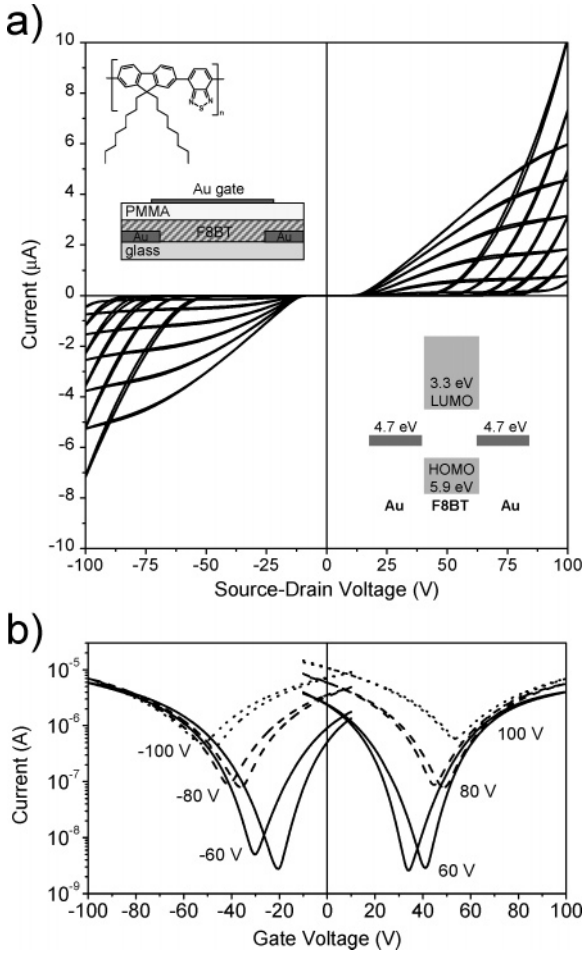

Figure 19. (a) Output characteristics of an ambipolar F8BT transistor with PMMA as the gate dielectric ($L = 10$ μm; $W/L = 500$) for different V_g (from 0 to −100 V and from 0 to 100 V in steps of 10 V). Inset top left: schematic device structure and chemical structure of F8BT. Inset bottom right: HOMO/LUMO levels compared to the work function of gold. **(**b**)** Transfer characteristics of the same transistor at different negative and positive V_{ds}. The saturation mobilities of holes and electrons for this device were 7.5×10^{-4} cm^2 V^{-1} s^{-1} and 8.5×10^{-4} cm^2 V^{-1} s^{-1}, respectively.

4.7. Modeling of Ambipolar FETs

Several groups have modeled the current−voltage characteristics of organic ambipolar transistors both numerically and analytically. The simplest treatment is based on the standard field-effect transistor equations introduced in section 2. Here, gate voltage-dependent mobilities and non-ohmic contacts are not taken into account. Considering the relative nature of potential in the transistor structure as described in section 4.2, one can define three distinct regimes depending on gate voltage, source−drain voltage, and threshold voltages for both holes and electrons ($V_{Th,h}$ and $V_{Th,e}$ with $V_{Th,h} < V_{Th,e}$): the unipolar linear regime, the unipolar saturation regime, and the ambipolar regime.[183]

For the first two, the following standard equations can be applied (here demonstrated for positive V_g and V_{ds}):

Unipolar linear regime $V_g > V_{Th,e}$ and

$$V_{ds} \leq (V_g - V_{Th,e}) \text{ and } V_{ds} \leq (V_g - V_{Th,h})$$

$$|I_{ds}| = \frac{WC_i}{L}\mu_e\left((V_g - V_{Th,e}) - \frac{V_{ds}}{2}\right)V_{ds} \quad (4.1)$$

Unipolar saturation regime $V_g > V_{Th,e}$ and

$$V_{ds} \geq (V_g - V_{Th,e}) \text{ and } V_{ds} \geq (V_g - V_{Th,h})$$

$$|I_{ds}| = \frac{WC_i}{2L}\mu_e(V_g - V_{Th,e})^2 \quad (4.2)$$

If $V_g < V_{Th,e}$ and $V_{ds} < (V_g - V_{Th,h})$, no charge transport occurs at all and $I_{ds} = 0$. When $V_g < V_{Th,e}$ and $V_{ds} \geq (V_g - V_{Th,h})$, only hole transport occurs, which again can be described by

$$|I_{ds}| = \frac{WC_i}{2L}\mu_h(V_{ds} - (V_g - V_{Th,h}))^2 \quad (4.3)$$

For a simple analytical expression for the ambipolar regime with $V_{ds} \geq (V_g - V_{Th,h})$ and $V_g > V_{Th,e}$, in which electron and hole accumulation layers of length L_e and L_h are present in the channel, we assume an infinite recombination rate of holes and electrons where the two channels meet. Thus, one can treat the transistor as consisting of a saturated electron and a saturated hole channel. Their individual lengths L_e and L_h add up to the total channel length L. As all injected holes and electrons have to recombine, the drain current equals the hole and the electron current ($I_{ds} = I_h = I_e$) for each channel.[183,245] From eq 4.2 for the individual saturated channels, we can thus derive

$$|I_{ds}| = \frac{WC_i}{2L}\{\mu_e(V_g - V_{Th,e})^2 + \mu_h(V_{ds} - (V_g - V_{Th,h}))^2\} \quad (4.4)$$

The ambipolar characteristics in Figure 12 were calculated on the basis of these equations and generally resemble observed current−voltage characteristics well. The position of the meeting point (recombination zone) $x_0 = L_e$ then is

$$x_0 = \frac{L(V_g - V_{Th,e})^2}{(V_g - V_{Th,e})^2 + \frac{\mu_h}{\mu_e}(V_{ds} - (V_g - V_{Th,h}))^2} \quad (4.5)$$

This model can be fitted to experimentally observed positions of the recombination zone in a long channel (L = 80 μm) ambipolar light-emitting transistor, e.g., in constant current mode[245] (see section 5.5) and shows how the position of the recombination zone depends on the applied gate and source-drain voltage, the threshold voltages and the mobility ratio. We emphasize that as long as the channel length is long compared to the spatial extent of the recombination zone in reality the model is not very sensitive to specific assumptions made about the processes in the recombination zone.

Smits et al. proposed a similar treatment using the variable range hopping model[63] to describe the charge transport in disordered organic materials, such as polymers. With this model, which also assumes an infinite recombination rate, they were able to fit experimental current−voltage data from ambipolar nickel dithiolene transistors[239] very well for a range of temperatures and voltages.[240] Another analytical model was recently proposed by Smith et al. that includes carrier trapping at low charge densities and produces current−voltage and potential characteristics in good agreement with experimental data.[185]

The limitation of these models is their simplifying assumption of an infinite recombination rate, which leads to a charge density of zero within the recombination zone. Assuming a finite recombination rate and thus a certain width of the recombination zone would be much more realistic. In that case, holes penetrate the electron channel and electrons penetrate the hole channel to a certain extent. The recombination zone is then a space-charge limited region, whose width is determined by the electric field associated with the potential drop across it. This would be similar to an LED with ohmic contacts for holes and electrons.

Numerical simulations of ambipolar transistors, on the other hand, can include Langevin recombination of holes and electrons as well as contact effects and reproduce the general shape of ambipolar transistor current−voltage characteristics reasonably well.[184,249] Paasch et al. found that the current−voltage characteristics depend critically on the employed electrode materials and the ratio of mobilities. On the basis of Langevin recombination, they also simulated the width of the recombination zone in a transistor with $L = 140$ μm and hole and electron mobilities in the range of 10^{-4} and 10^{-3} cm^2 V^{-1} s^{-1}, respectively, to be several micrometers.[184]

5. Light-Emitting Field-Effect Transistors

5.1. Motivation

For any semiconductor technology, one of the key issues is to realize devices that integrate electronic functions (e.g., transistors) with optical functions (e.g., light sources and light detectors). Light-emitting field-effect transistors (LFETs) provide a very simple integration scheme for combining the switching properties of transistors with the emission properties of light-emitting diodes (LEDs).

As discussed in section 4.3, ambipolar amorphous silicon transistors are not suitable for light emission due to the indirect band gap of bulk silicon. Some progress to produce silicon light-emitting transistors was nevertheless made with pulsed FET-like devices that contained silicon nanocrystals as emitters by injecting and trapping first electrons and then holes in the channel region.[250] Using quantum mechanical confinement in ultrathin single-crystal silicon and thus quasidirect band gap character, Saito et al. fabricated a silicon light-emitting transistor based on a planar doped pn-junction.[251] Furthermore, inorganic near-infrared light-emitting transistors based on a InGaP/GaAs heterojunction were recently demonstrated by Feng et al.[252] Here, a heterojunction bipolar transistor (HBT) emits light from the graded base layer of InGaP/GaAs. Enhanced radiative recombination and gigahertz operation were realized by incorporating InGaAs quantum wells.[252] Ambipolar carbon nanotube FETs show polarized infrared light emission in the infrared but require a high degree of processing, including e-beam lithography and high temperatures.[197,198]

Organic semiconductors seem like an ideal candidate for light emission applications. Many small molecule and conjugated polymer semiconductors show very high photoluminescence (PL) and electroluminescence (EL) efficiencies

over the whole visible spectrum as well as decent charge transport properties, which enable their use in light-emitting diodes.[253−256]

In recent years, many research groups have worked on realizing light emission from organic field-effect transistors. Ambipolar organic FETs seemed predestined for light emission, as proposed by Dodabalapur et al.,[257] as they can provide an effective pn-junction within the transistor channel and thus radiative recombination of holes and electrons. But the first results were reported unexpectedly for unipolar organic transistors,[258] and many examples of that kind have been demonstrated since then.[259−271] Another approach involved a pre-engineered pn-junction within the channel of an organic transistor.[272] Most of the scientifically and technologically interesting properties that make light-emitting transistors desirable are, however, only present in ambipolar light-emitting transistors. These include control over the position of the emission zone, emission far away from metal electrodes, high current densities, low charge concentration within the emission zone, and perfectly balanced hole and electron currents. These properties could make light-emitting transistors attractive for novel integrated electro-optical switches and, potentially, electrically pumped lasers. They also offer a convenient planar structure with which to investigate recombination physics in organic semiconductors using spatially resolving probes.

5.2. Unipolar Light-Emitting FETs

The first light-emitting transistor based on an organic semiconductor was reported in 2003 by Hepp et al. They found light emission in a tetracene FET that only showed p-channel behavior.[258] This was unexpected because both holes and electrons have to be present in the channel in order to recombine and thus form an exciton that can relax radiatively. The employed structure of bottom Cr/Au electrodes also seemed ill-suited for electron injection into the LUMO level of tetracene (2.4 eV). A closer look revealed that light emission took place exclusively at the edges of the drain electrodes and not from within the channel. This behavior was attributed to an undercut of the etched electrodes, which led to a device structure that could be compared to a field-effect transistor combined with an LED that operated at high fields. This device structure was also successfully employed to realize unipolar light-emitting polymer transistors based on F8.[259] Santato et al. later found that the electrode undercut was not necessary to achieve light emission in tetracene transistors with Au electrodes,[260,262,263] but they proposed a model where electrons tunnel from the drain electrode into the channel through a triangular tunneling barrier generated by a steep voltage drop at that contact, as shown in Figure 20. This approach also worked for other materials, such as thiophenes.[261]

Electron injection into unipolar p-type transistors can, of course, be improved by using composite electrodes with one metal being gold the other having a lower work function, such as, for example, aluminum. Sakanoue et al. found a dependence of the emission efficiency on the work function of the injecting electrodes for MEH-PPV light-emitting transistors with Cr/Au and Al/Au bottom electrodes.[269] Oyamada et al. demonstrated that shorter channels (as short as 0.4 μm) and thus higher electric fields helping charge injection combined with a range of suitable electrode materials enabled more efficient light emission in unipolar transistors with a wide range of semiconducting and electroluminescent organics.[265−267] The highest external quantum efficiency of 0.8% was observed for a short channel transistor (L = 0.4 μm) with tetraphenylpyrene (TPPy) doped with rubrene (PL efficiency ~ 100%) as the active layer. These

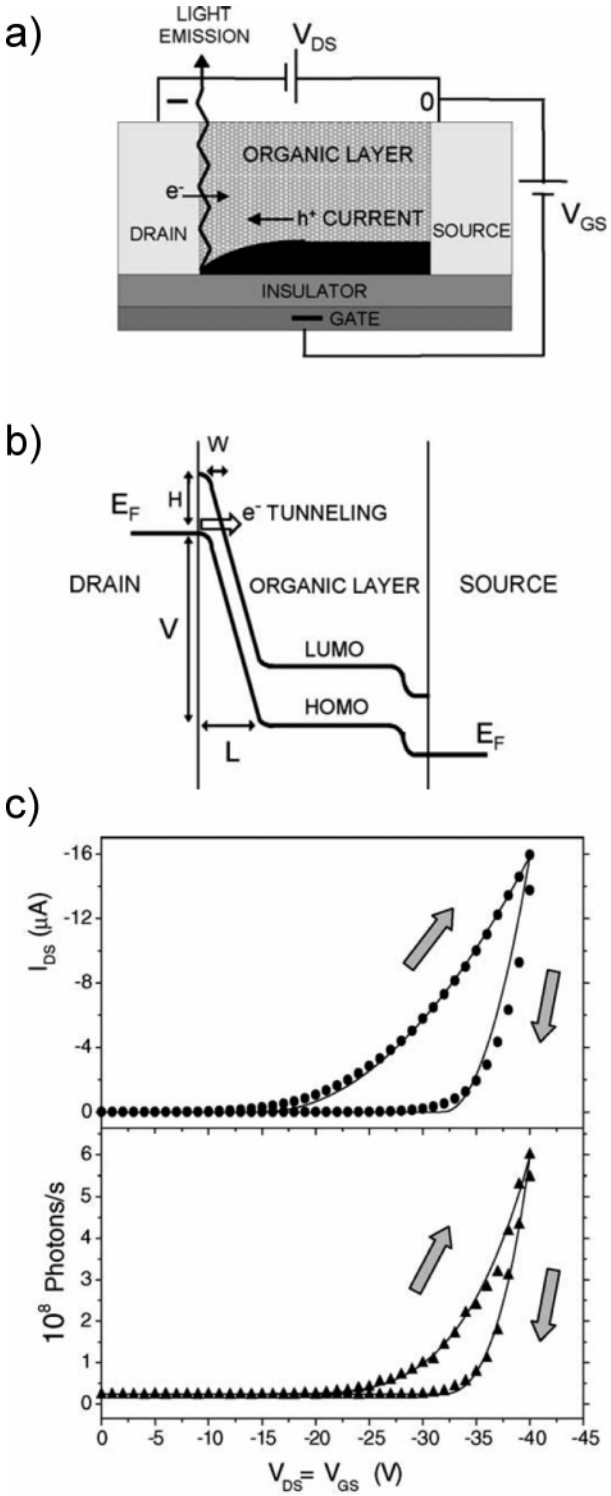

Figure 20. (a) Working principle of a unipolar organic light-emitting transistor. The main electronic processes taking place when the device is operated in standard p-type mode are indicated. **(**b**)** Energy level diagram showing the mechanism for electron injection from gold into the organic material at the drain electrode. **(**c**)** Experimental (symbols) and simulated (solid lines) hysteresis loops for drain current and electroluminescence intensity. Hysteresis is due to an increase of the gate voltage threshold during device operation. Reprinted from ref 260, Copyright 2004, with permission from Elsevier.

short channel transistors were, in their characteristics, similar to lateral LEDs, and fields comparable to those in standard sandwich LEDs were applied.

The unipolar character of all these devices probably explains the observed low external efficiencies. Recombination is limited by the injection of electrons, which is insufficient, and thus, the majority of holes that cross the channel do not contribute to light emission.

In order to improve electron injection further without impeding hole injection, several research groups used asymmetric source−drain electrodes with a gold electrode for hole injection and a low work function metal electrode for electron injection. This way, light emission could be achieved in vacuum sublimed tetracene,[271] solution-processed conjugated polymer (SuperYellow),[270] and single-crystal (thiophene/phenylene co-oligomer BP3T)[268] transistors. But despite the optimal electron injection, no n-channel behavior was observed and light emission took place only at the drain electrodes, identical to the results for the above-described devices with only gold electrodes.

5.3. Light-Emitting FETs with a pn-Junction

The restriction of light emission to the edge of the drain electrode and low quantum efficiencies are the major drawbacks of unipolar light-emitting transistors. In order to move the recombination zone into the transistor channel, de Vusser et al. proposed a new device structure that involves a pn-junction of a p-channel material with low electron affinity (OOctyl-OPV5) and a n-channel material with high electron affinity (PTCDI-$C_{13}H_{27}$) in the channel region.[272] This was accomplished by angled evaporation of the two components. The transistor then essentially operates with a hole source and an electron source. Recombination of holes and electrons takes place where the two components overlap, which is visualized by green light emission from that region. At least theoretically, a limited control of the recombination zone position through the applied gate and source−drain voltage is possible in this device.

5.4. Multicomponent Ambipolar Light-Emitting FETs

As explained in sections 4.2 and 4.7, separate hole and electron channels should coexist in truly ambipolar transistors. Where the two channels meet, charge recombination and light emission are expected to take place. As the relative length of the two channels depends on the potential profile in the channel and thus on the gate and source−drain voltages, the position of the emission zone should be movable from one electrode through the channel to the other electrode. Observing this behavior would be the ultimate experimental proof of the concept of two channels in series and the ambipolar nature of charge transport. Due to the effective pn-junction within the channel and complete recombination of holes and electrons, the quantum efficiency of ambipolar light-emitting FETs should also be much higher than that of unipolar light-emitting FETs.

Rost et al. reported the first ambipolar light-emitting transistor based on coevaporated PTCDI-$C_{13}H_{27}$ and α-quinquethiophene (α-5T).[211] Light emission was observed for several voltage conditions, and the light intensity was proportional to the drain current. However, the position of the emission zone was not reported. Loi et al. later found that light emission from this blend depends on the ratio of PTCDI-$C_{13}H_{27}$ to α-5T.[212] When there is an excess of α-5T, ambipolar transport takes place but no light is detected, which is attributed to quenching of PTCDI-$C_{13}H_{27}$ excitons upon interaction with α-5T. For an excess of PTCDI-$C_{13}H_{27}$, on the other hand, only n-channel behavior is observed. Nevertheless, light is emitted from the transistor. Both ambipolar transport and light emission are achieved for a balanced ratio of the two components.

Dinelli et al. reported that bilayers of α,ω-dihexylquarterthiophene (DH4T) and PTCDI-$C_{13}H_{27}$ show good ambipolar transistor behavior and light emission.[204] However, light emission took place only in the unipolar regime, which indicates that one should consider the pn-junction underneath the electrodes as the source of emission instead of a recombination zone arising from hole and electron channels in series.

5.5. Single-Component Ambipolar Light-Emitting FETs

As shown in section 5.2, light emission from a transistor is not always coincident with ambipolar transport characteristics, and even some ambipolar transistors show light emission only in the unipolar regime. Furthermore, the introduced model of a hole and an electron channel that meet

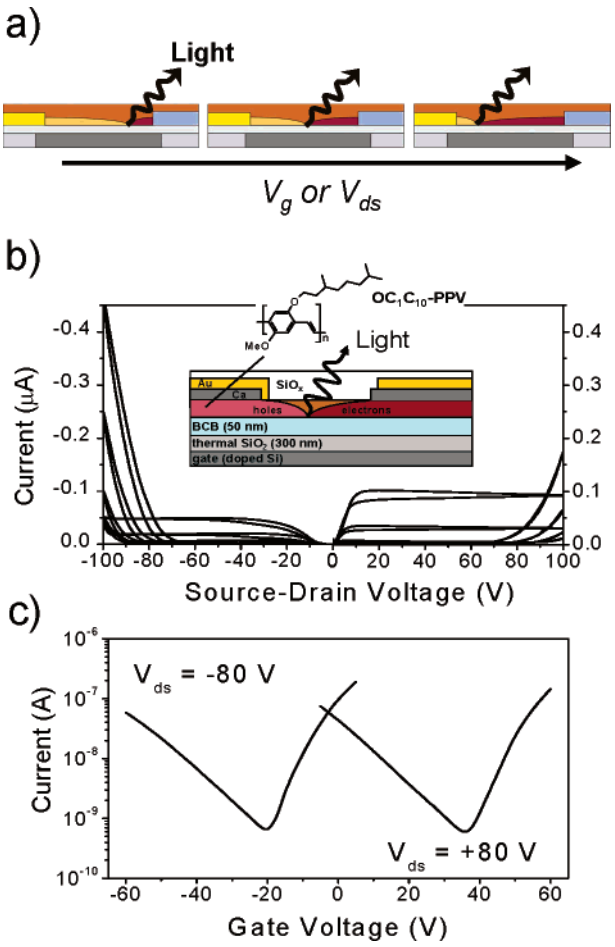

Figure 21. (a) Schematic working principle of ambipolar light-emitting transistors. Light is emitted where the hole channel and the electron channel meet. The position of this emission zone depends on the applied voltages. **(**b**)** Output characteristic of an ambipolar OC_1C_{10}-PPV light-emitting transistor with V_g from 0 to −60 V and 0 to 60 V in steps of 10 V. Inset: schematic device structure and working principle. **(**c**)** Transfer characteristics of the same transistor for V_{ds} = 80 V and −80 V. Adapted from ref 245.

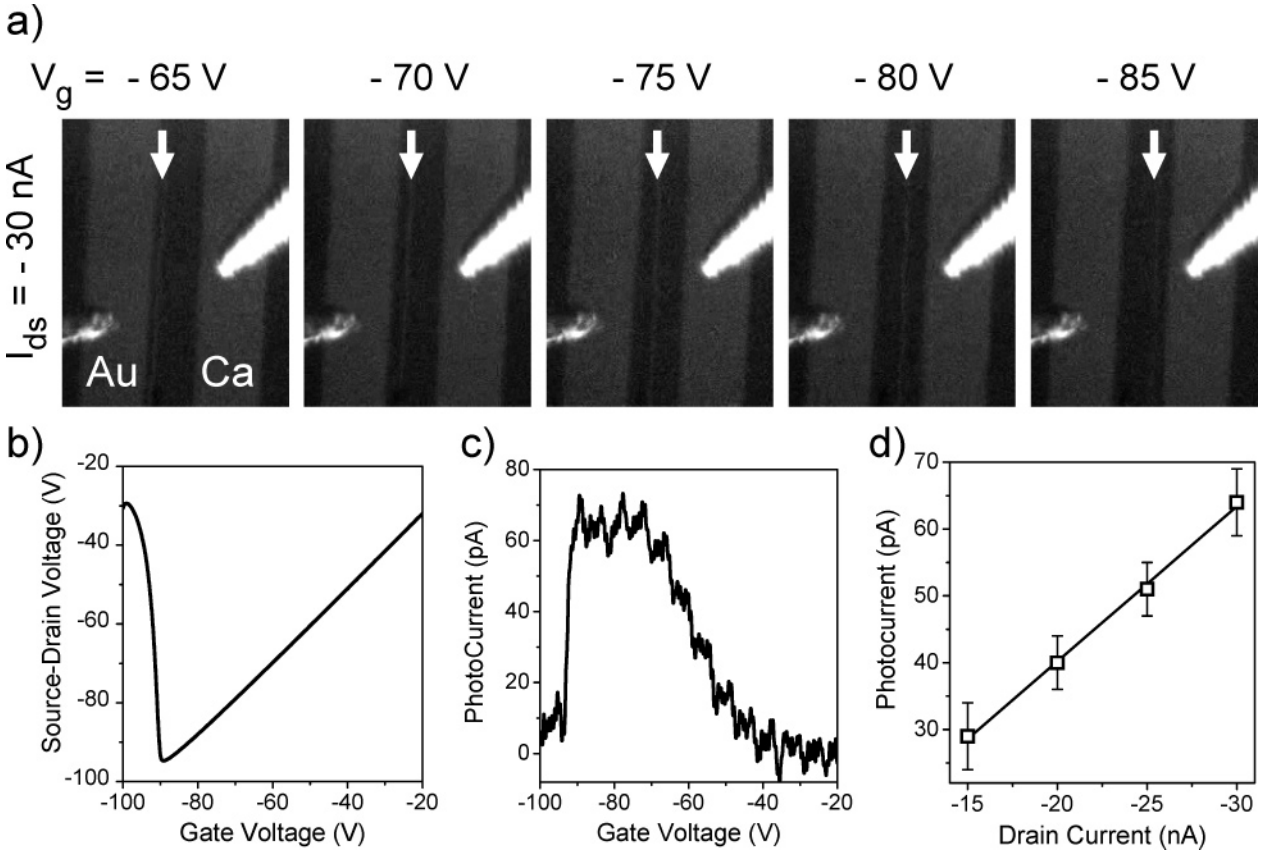

Figure 22. (a) Optical images of light emission from an OC_1C_{10}-PPV transistor at a constant drain current of −30 nA during a gate voltage sweep. The emission zone moves from the gold electrode (left) to the calcium electrode (right) with increasing $-V_g$. **(**b**)** V_{ds} as a function of V_g for a fixed drain current of −30 nA. **(**c**)** Corresponding photocurrent during the forward scan. **(**d**)** Average photocurrent at plateau versus drain current (squares), and linear fit (solid line). The error bars indicate the standard deviation from the average value. Adapted from ref 245.

within the channel of an ambipolar transistor cannot be proven by these results. For blend devices, one could, for example, assume different percolation paths for holes and electrons and thus, in fact, two parallel channels and emission at the heterojunctions. An unambiguous experimental proof for the model of two channels in series is the visual resolution of the recombination and, thus, emission zone, which is not only located at the drain electrode but in fact can be moved through the whole channel by changing the applied voltages as schematically shown in Figure 21a.

As shown in section 4.6.5 for P3HT transistors, ambipolar behavior is achievable for conjugated polymers when trap-free dielectrics in combination with a high and a low work function metal electrode are used. But P3HT has a very low PL efficiency, and thus, possible light emission would be difficult to observe. Replacing P3HT with a semiconducting polymer with a higher PL efficiency should yield visible light emission. The PPV derivative OC_1C_{10}-PPV emits orange/red light (emission maximum around 650 nm) and exhibits a PL efficiency of approximately 10%,[273,274] which makes it a good candidate for a light-emitting transistor. Figure 21b (inset) shows a schematic transistor structure with OC_1C_{10}-PPV as the semiconducting and emissive layer and Ca and Au as electron and hole injecting electrodes, respectively. Cured BCB serves again as a buffer dielectric preventing trapping and enabling transport of electrons.[245] Good ambipolar output and transfer characteristics are evident (Figure 21b and c). The electron and hole mobilities in the saturation regime are on average 3×10^{-3} cm^2 V^{-1} s^{-1} and 6×10^{-4} cm^2 V^{-1} s^{-1}, respectively.

When the device is biased in the ambipolar regime, light emission from the channel becomes visible. The recombination zone in this ambipolar transistor, visible as a narrow bright line parallel to the electrodes, is movable from one electrode through the channel to the other electrode by changing the applied voltages and thus changing the potential profile. This is demonstrated in Figure 22a for a gate voltage sweep in constant current mode. The drain current is fixed at −30 nA, and the gate voltage is scanned from 0 to −100 V while the source−drain voltage is adjusted accordingly (Figure 22b). At low $-V_g$ and high $-V_{ds}$, the channel is dominated by electrons and no light is emitted. However, when $-V_g$ increases, holes start being injected and light becomes visible at the edge of the Au electrode. As $-V_g$ further increases, the emission zone moves through the channel until it reaches the Ca electrode. Now the channel is dominated by holes and the light vanishes. The measured half-maximum width of the emission zone of about 2 μm might be limited by the resolution of the camera but clearly proves the existence of a defined recombination zone. The intensity of the emitted light remains constant while the emission zone moves through the channel but is reduced when emission takes place close to one of the electrodes (Figure 22c). When the drain current is increased, the light intensity increases proportionally (Figure 22d). One can assume that while the emission zone is located within the channel, all holes and electrons recombine even for finite recombination rates, as it is unlikely that a charge carrier could cross several micrometers of an oppositely charged accumulation layer. The injected hole current I_h must hence

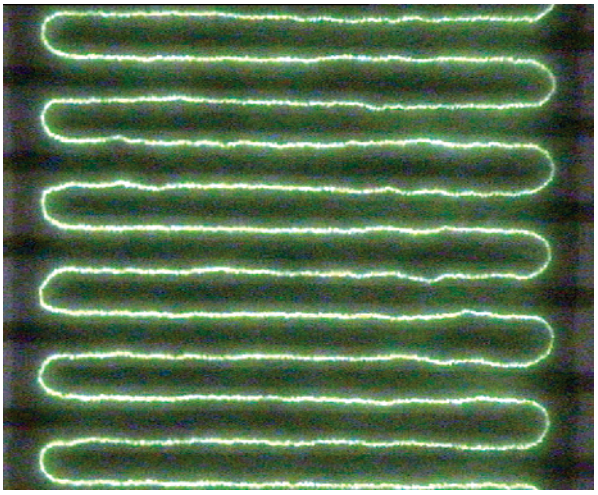

Figure 23. Optical image of the light emission from an ambipolar F8BT transistor with bottom contact gold electrodes and PMMA as the gate dielectric seen through the gold top gate electrode. Channel length $L = 20$ μm; applied bias $V_g = 50$ V; $V_{ds} = 100$ V.

be exactly equal to the injected electron current I_e, which is the drain current $I_d = I_h = I_e$. Thus, the emitted light is directly proportional to the drain current and the external quantum efficiency can be calculated to be 0.35%. This translates into an approximate internal quantum efficiency of 2 ± 1%, which is similar to that of light-emitting diodes based on OC_1C_{10}-PPV.[273,274] This is surprising because the current density in the light-emitting FET (1−10 A/cm^2, calculated assuming a 1−2 nm thick accumulation layer) is much higher than current densities in standard LEDs (10^{-3}−10^{-2} A/cm^2, when operated at the point of maximum quantum efficiency). The quantum efficiency for emission close to the electrodes is reduced, probably due to charge carriers escaping into the electrodes without recombination or quenching of excitons by the metal. Similar emission behavior has been observed for ambipolar FETs based on the PPV derivative SuperYellow by Swenson et al.[246]

The observation of a narrow zone of light emission that moves through the channel with changing voltages visualizes and unambiguously proves the existence of two separate channels of holes and electrons in series within the channel of a transistor in the ambipolar regime. The ambipolar transistor models proposed by Schmechel et al.[183] and Smits et al.[240] are thus physically correct and can be applied to model the position of the emission zone in ambipolar transistors.

As described in section 4.6.6, bottom contact/top gate F8BT transistors show very good ambipolar characteristics with hole and electron mobilities of about 8×10^{-4} cm^2 V^{-1} s^{-1} (see Figure 19). F8BT is a an efficient green emitter with photoluminescence efficiencies in solid films of 50−60%[275] and is often used in polymer blend LEDs.[172−174] When operated in the ambipolar regime, F8BT transistors show stable, bright green light emission from within the channel,[247] as shown in Figure 23 for a transistor with interdigitated electrodes with a channel length of 20 μm. The non-uniformity of the emission zone in this device highlights the microscopic, polycrystalline structure of the F8BT film. In the same manner as in the OC_1C_{10}-PPV transistors, the emission zone can be moved through the channel by changing the applied voltages. Figure 24a shows the position of the emission zone within a 100 μm channel during a

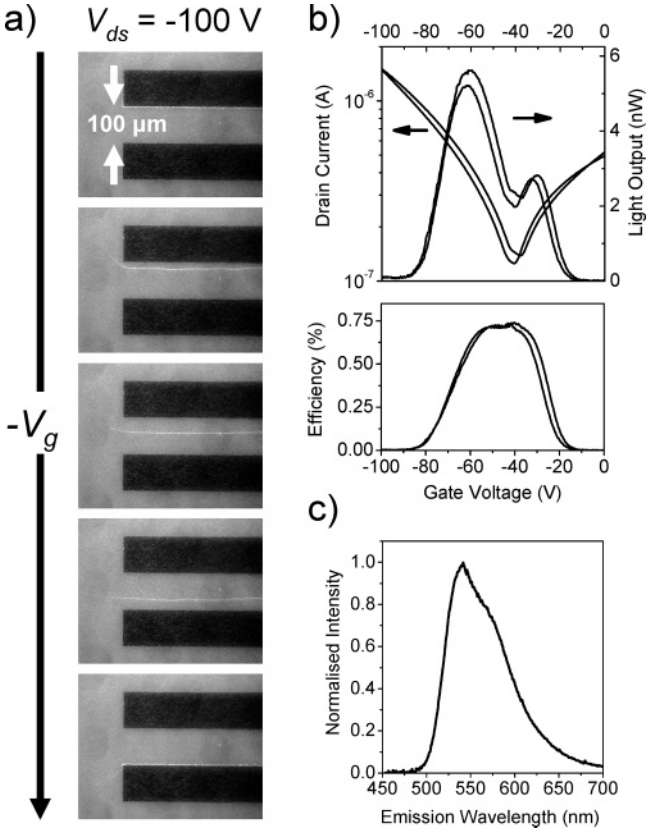

Figure 24. (a) Optical images of the recombination and emission zones of a F8BT transistor with PMMA as the dielectric ($L = 100$ μm; $W = 4$ mm) during a transfer scan at $V_{ds} = -100$ V and different V_g (between approximately −35 and −50 V). **(b)** Transfer characteristics, corresponding light output, and external quantum efficiency of a F8BT transistor with T-shaped electrodes ($L = 75$ μm; $W = 4$ mm) and PMMA as the gate dielectric. The emission efficiency reaches a maximum plateau (0.75%) when the recombination zone is expected to be located within the channel, and thus, all injected holes and electrons must recombine. **(c)** Electroluminescence spectrum of a light-emitting F8BT transistor. Parts b and c are reprinted and adapted with permission from ref 247. Copyright 2006 Wiley-VCH Verlag GmbH & Co. KGaA.

transfer scan with fixed $V_{ds} = -100$ V and changing V_g. The visible extension of emission outside the channel region visualizes the stray fields at the edges of a transistor with a gate electrode not confined to the immediate channel region. Figure 24b shows the transfer and corresponding light output characteristics of a F8BT light-emitting FET (LFET) with a channel length of 75 μm and width of 4 mm. Two peaks in the light output versus gate voltage characteristics are apparent when either hole or electron current dominates. A local minimum occurs when the drain current reaches a minimum. Looking at the external quantum efficiency, however, we find a global maximum plateau around the drain current minimum. This corresponds to the gate voltage region where the emission zone is positioned within the channel. In this regime, all injected holes and electrons have to recombine and a perfect balance of electron and hole currents is reached. The maximum external quantum efficiency of this device is 0.75%, which is somewhat better than that of corresponding single-layer F8BT light-emitting diodes (∼0.5%), despite partial reflection and absorption of the emitted light by the gold gate. The highest current densities achieved in the ambipolar regime are on the order of 20 A/cm^2 for transistors with a channel length of 5 μm. The emission spectrum of the F8BT LFET (Figure 24c) is almost

indistinguishable from that of corresponding single-layer F8BT LEDs. The emission characteristics are thus not notably affected by the special properties of light-emitting transistors such as high electric fields across the emission zone, the presence of the gate dielectric adjacent to the recombination zone, and high current densities in the accumulation layer of the FET.

Ambipolar light-emitting transistors with resolved and movable light emission are not only an unambiguous proof of the concept of hole and electron channels in series in ambipolar transistors and the intrinsic ambipolar character of organic semiconductors but also enable new ways of studying emission physics of organic materials as well as new optoelectronic devices. The planar structure of light-emitting transistors will allow using local microscopy techniques such as scanning near field microscopy (SNOM), confocal microscopy, and scanning Kelvin probe microscopy (SKPM) to resolve the emission and potential profiles within the channel, which is not possible in standard LED structures. Furthermore, control over the position of the recombination zone could lead to novel electro-optical switches by incorporating waveguide structures into the channel region. By reducing charge carrier densities and positioning the emission zone far away from any metal electrode, light-emitting FETs may provide a means to reduce optical loss mechanisms, which have so far prevented the realization of electrically pumped organic lasers based on standard LED structures.[276,277]

6. Conclusions and Outlook

Over the past few years, tremendous progress has been made in understanding both hole and electron transport in organic semiconductors. As the purity and availability of semiconducting materials in their various forms as polymers, thin films, and single crystals have improved, it has become clear that many organic semiconductors are indeed clean, intrinsic semiconductors that allow formation of both electron and hole accumulation layers in organic field-effect transistors, as suggested by theoretical calculations for a long time. In other words, in spite of their sometimes disordered nature, the density of states in the band gap is sufficiently small that the quasi-Fermi level can be swept all the way from the HOMO to the LUMO states to invert the channel, as is possible in many crystalline inorganic semiconductors. The prerequisites to experimentally observing n-channel and ambipolar transport in organic semiconductors with low electron affinities (EA < 3.5 eV) are high purity, appropriate injection electrodes, trap-free gate dielectrics, and testing under inert conditions.

The ability to observe both electron and hole transport in organic semiconductors opens up new opportunities for both scientific studies and technological applications of these materials. Both n-channel and ambipolar FETs enable new device applications based on organic complementary circuits and light-emitting transistors. There are still a number of scientific and technological challenges that will need to be addressed. It is not yet proven that n-channel and ambipolar organic FETs will be able to achieve the same operational and environmental stability that has recently been demonstrated for p-channel organic FETs.[125,127] Those FETs can be operated without encapsulation in air and light without significant degradation and threshold voltage changes. To achieve similarly impressive performance with n-channel FETs will be more challenging, partly due to the limited electrochemical stability of the radical anions in many organic semiconductors. However, a number of materials with encouraging stabilities have been reported already,[224,239] and this research direction is receiving increasing attention. Further progress over the next couple of years may solve these issues.

From a scientific point of view, n-channel and ambipolar FETs open up new opportunities for a better understanding of the device physics of organic semiconductors. Of particular importance for basic scientific studies are single-component materials and device configurations that allow realization of ambipolar transport, because they enable direct comparison of the relative transport properties of electrons and holes in a single device. In general, studies of n-channel and ambipolar FETs will close some of the gaps in understanding how the transport properties of organic diodes (LEDs and photodiodes) relate to those of organic FETs, and will draw a more unified picture of the physics of organic electronic devices.

7. Acknowledgments

The authors thank C. L. Donley, J. S. Kim, R. H. Friend, P. K. H. Ho, L. L. Chua, T. R. Richards, and C. R. Newman for useful discussions. J.Z. thanks the Gates Cambridge Trust for funding. For our work on n-type and ambipolar organic FETs, we acknowledge funding from the Engineering and Physical Sciences Research Council.

8. References

(1) Ebisawa, F.; Kurokawa, T.; Nara, S. *J. Appl. Phys.* **1983**, *54*, 3255.
(2) Tsumura, A.; Koezuka, H.; Ando, T. *Appl. Phys. Lett.* **1986**, *49*, 1210.
(3) Assadi, A.; Svensson, C.; Willander, M.; Inganas, O. *Appl. Phys. Lett.* **1988**, *53*, 195.
(4) Kudo, K.; Yamashina, M.; Moriizumi, T. *Jpn. J. Appl. Phys.* **1984**, *23*, 130.
(5) Horowitz, G.; Fichou, D.; Peng, X. Z.; Xu, Z. G.; Garnier, F. *Solid State Commun.* **1989**, *72*, 381.
(6) Rotzoll, R.; Mohapatra, S.; Olariu, V.; Wenz, R.; Grigas, M.; Dimmler, K.; Shchekin, O.; Dodabalapur, A. *Appl. Phys. Lett.* **2006**, *88*, Art. No. 123502.
(7) Baude, P. F.; Ender, D. A.; Haase, M. A.; Kelley, T. W.; Muyres, D. V.; Theiss, S. D. *Appl. Phys. Lett.* **2003**, *82*, 3964.
(8) Rogers, J. A.; Bao, Z.; Baldwin, K.; Dodabalapur, A.; Crone, B.; Raju, V. R.; Kuck, V.; Katz, H.; Amundson, K.; Ewing, J.; Drzaic, P. *Proc. Natl. Acad. Sci. U.S.A.* **2001**, *98*, 4835.
(9) Sirringhaus, H.; Kawase, T.; Friend, R. H. *MRS Bull.* **2001**, *26*, 539.
(10) Gelinck, G. H.; Huitema, H. E. A.; van Veenendaal, E.; Cantatore, E.; Schrijnemakers, L.; van der Putten, J.; Geuns, T. C. T.; Beenhakkers, M.; Giesbers, J. B.; Huisman, B. H.; Meijer, E. J.; Benito, E. M.; Touwslager, F. J.; Marsman, A. W.; van Rens, B. J. E.; de Leeuw, D. M. *Nat. Mater.* **2004**, *3*, 106.
(11) Zhou, L. S.; Wanga, A.; Wu, S. C.; Sun, J.; Park, S.; Jackson, T. N. *Appl. Phys. Lett.* **2006**, *88*, Art. No. 083502.
(12) Lee, S.; Koo, B.; Park, J. G.; Moon, H.; Hahn, J.; Kim, J. M. *MRS Bull.* **2006**, *31*, 455.
(13) Burns, S. E.; Reynolds, K.; Reeves, W.; Banach, M.; Brown, T.; Chalmers, K.; Cousins, N.; Etchells, M.; Hayton, C.; Jacobs, K.; Menon, A.; Siddique, S.; Too, P.; Ramsdale, C.; Watts, J.; Cain, P.; von Werne, T.; Mills, J.; Curling, C.; Sirringhaus, H.; Amundson, K.; McCreary, M. D. *J. Soc. Inf. Disp.* **2005**, *13*, 583.
(14) Gelinck, G. H.; Huitema, H. E. A.; van Mil, M.; van Veenendaal, E.; van Lieshout, P. J. G.; Touwslager, F.; Patry, S. F.; Sohn, S.; Whitesides, T.; McCreary, M. D. *J. Soc. Inf. Disp.* **2006**, *14*, 113.
(15) Blochwitz, J.; Pfeiffer, M.; Fritz, T.; Leo, K. *Appl. Phys. Lett.* **1998**, *73*, 729.
(16) Maennig, B.; Pfeiffer, M.; Nollau, A.; Zhou, X.; Leo, K.; Simon, P. *Phys. Rev. B* **2001**, *64*, 195208.
(17) Nollau, A.; Pfeiffer, M.; Fritz, T.; Leo, K. *J. Appl. Phys.* **2000**, *87*, 4340.

(18) Bernius, M. T.; Inbasekaran, M.; O'Brien, J.; Wu, W. S. *Adv. Mater.* **2000**, *12*, 1737.
(19) Becker, H.; Spreitzer, H.; Kreuder, W.; Kluge, E.; Schenk, H.; Parker, I.; Cao, Y. *Adv. Mater.* **2000**, *12*, 42.
(20) Jurchescu, O. D.; Baas, J.; Palstra, T. T. M. *Appl. Phys. Lett.* **2004**, *84*, 3061.
(21) Chua, L. L.; Zaumseil, J.; Chang, J. F.; Ou, E. C. W.; Ho, P. K. H.; Sirringhaus, H. R.; Friend, H. *Nature* **2005**, *434*, 194.
(22) Dimitrakopoulos, C. D.; Malenfant, P. R. L. *Adv. Mater.* **2002**, *14*, 99.
(23) Veres, J.; Ogier, S.; Lloyd, G.; de Leeuw, D. *Chem. Mat.* **2004**, *16*, 4543.
(24) Facchetti, A.; Yoon, M. H.; Marks, T. J. *Adv. Mater.* **2005**, *17*, 1705.
(25) Klauk, H.; Gundlach, D. J.; Nichols, J. A.; Jackson, T. N. *IEEE Trans. Electron Devices* **1999**, *46*, 1258.
(26) Majewski, L. A.; Schroeder, R.; Grell, M. *Appl. Phys. Lett.* **2004**, *85*, 3620.
(27) Tate, J.; Rogers, J. A.; Jones, C. D. W.; Vyas, B.; Murphy, D. W.; Li, W. J.; Bao, Z. A.; Slusher, R. E.; Dodabalapur, A.; Katz, H. E. *Langmuir* **2000**, *16*, 6054.
(28) Cai, X. Y.; Burand, M. W.; Newman, C. R.; da Silva, D. A.; Pappenfus, T. M.; Bader, M. M.; Bredas, J. L.; Mann, K. R.; Frisbie, C. D. *J. Phys. Chem. B* **2006**, *110*, 14590.
(29) Kawase, T.; Shimoda, T.; Newsome, C.; Sirringhaus, H.; Friend, R. H. *Thin Solid Films* **2003**, *438*, 279.
(30) Sirringhaus, H.; Kawase, T.; Friend, R. H.; Shimoda, T.; Inbasekaran, M.; Wu, W.; Woo, E. P. *Science* **2000**, *290*, 2123.
(31) Sele, C. W.; von Werne, T.; Friend, R. H.; Sirringhaus, H. *Adv. Mater.* **2005**, *17*, 997.
(32) Lefenfeld, M.; Blanchet, G.; Rogers, J. A. *Adv. Mater.* **2003**, *15*, 1188.
(33) Makela, T.; Jussila, S.; Kosonen, H.; Backlund, T. G.; Sandberg, H. G. O.; Stubb, H. *Synth. Met.* **2005**, *153*, 285.
(34) Lee, K. S.; Smith, T. J.; Dickey, K. C.; Yoo, J. E.; Stevenson, K. J.; Loo, Y. L. *Adv. Funct. Mater.* **2006**, *16*, 2409.
(35) Kobayashi, S.; Nishikawa, T.; Takenobu, T.; Mori, S.; Shimoda, T.; Mitani, T.; Shimotani, H.; Yoshimoto, N.; Ogawa, S.; Iwasa, Y. *Nat. Mater.* **2004**, *3*, 317.
(36) Pernstich, K. P.; Haas, S.; Oberhoff, D.; Goldmann, C.; Gundlach, D. J.; Batlogg, B.; Rashid, A. N.; Schitter, G. *J. Appl. Phys.* **2004**, *96*, 6431.
(37) Chua, L. L.; Ho, P. K. H.; Sirringhaus, H.; Friend, R. H. *Appl. Phys. Lett.* **2004**, *84*, 3400.
(38) Frank, D. J.; Dennard, R. H.; Nowak, E.; Solomon, P. M.; Taur, Y.; Wong, H. S. P. *Proc. IEEE* **2001**, *89*, 259.
(39) Sze, S. M. *Semiconductor Devices—Physics and Technology*; John Wiley and Sons, Inc.: New York, 2002.
(40) Austin, M. D.; Chou, S. Y. *Appl. Phys. Lett.* **2002**, *81*, 4431.
(41) Chabinyc, M. L.; Lu, J. P.; Street, R. A.; Wu, Y. L.; Liu, P.; Ong, B. S. *J. Appl. Phys.* **2004**, *96*, 2063.
(42) Tulevski, G. S.; Nuckolls, C.; Afzali, A.; Graham, T. O.; Kagan, C. R. *Appl. Phys. Lett.* **2006**, *89*, Art. No. 183101.
(43) Haddock, J. N.; Zhang, X. H.; Zheng, S. J.; Zhang, Q.; Marder, S. R.; Kippelen, B. *Org. Electron.* **2006**, *7*, 45.
(44) Kagan, C. R.; Afzali, A.; Martel, R.; Gignac, L. M.; Solomon, P. M.; Schrott, A. G.; Ek, B. *Nano Lett.* **2003**, *3*, 119.
(45) Salleo, A.; Street, R. A. *J. Appl. Phys.* **2003**, *94*, 471.
(46) Rep, D. B. A.; Morpurgo, A. F.; Sloof, W. G.; Klapwijk, T. M. *J. Appl. Phys.* **2003**, *93*, 2082.
(47) Salleo, A.; Street, R. A. *Phys. Rev. B* **2004**, *70*, 235324.
(48) Street, R. A.; Salleo, A.; Chabinyc, M.; Paul, K. *J. Non-Cryst. Solids* **2004**, *338−40*, 607.
(49) Ng, T. N.; Marohn, J. A.; Chabinyc, M. L. *J. Appl. Phys.* **2006**, *100*, Art. No. 084505.
(50) Kagan, C. R.; Afzali, A.; Graham, T. O. *Appl. Phys. Lett.* **2005**, *86*, 193505.
(51) Schroeder, R.; Majewski, L. A.; Grell, M. *Adv. Mater.* **2004**, *16*, 633.
(52) Naber, R. C. G.; Tanase, C.; Blom, P. W. M.; Gelinck, G. H.; Marsman, A. W.; Touwslager, F. J.; Setayesh, S.; de Leeuw, D. M. *Nat. Mater.* **2005**, *4*, 243.
(53) Hoshino, S.; Yoshida, M.; Uemura, S.; Kodzasa, T.; Takada, N.; Kamata, T.; Yase, K. *J. Appl. Phys.* **2004**, *95*, 5088.
(54) Russell, D. M.; Kugler, T.; Newsome, C. J.; Li, S. P.; Ishida, M.; Shimoda, T. *Synth. Met.* **2006**, *156*, 769.
(55) Arias, A. C.; Endicott, F.; Street, R. A. *Adv. Mater.* **2006**, *18*, 2900.
(56) Street, R. A.; Salleo, A. *Appl. Phys. Lett.* **2002**, *81*, 2887.
(57) Gundlach, D. J.; Zhou, L.; Nichols, J. A.; Jackson, T. N.; Necliudov, P. V.; Shur, M. S. *J. Appl. Phys.* **2006**, *100*, Art. No. 024509.
(58) Hill, I. G. *Appl. Phys. Lett.* **2005**, *87*, Art. No. 163505.
(59) Newman, C. R.; Chesterfield, R. J.; Panzer, M. J.; Frisbie, C. D. *J. Appl. Phys.* **2005**, *98*, 084506.
(60) Lei, C. H.; Das, A.; Elliott, M.; Macdonald, J. E.; Turner, M. L. *Synth. Met.* **2004**, *145*, 217.
(61) Roichman, Y.; Tessler, N. *Appl. Phys. Lett.* **2002**, *80*, 151.
(62) Bassler, H. *Phys. Status Solidi B* **1993**, *175*, 15.
(63) Vissenberg, M.; Matters, M. *Phys. Rev. B* **1998**, *57*, 12964.
(64) Meijer, E. J.; Tanase, C.; Blom, P. W. M.; van Veenendaal, E.; Huisman, B. H.; de Leeuw, D. M.; Klapwijk, T. M. *Appl. Phys. Lett.* **2002**, *80*, 3838.
(65) Tanase, C.; Meijer, E. J.; Blom, P. W. M.; de Leeuw, D. M. *Org. Electron.* **2003**, *4*, 33.
(66) Tanase, C.; Meijer, E. J.; Blom, P. W. M.; de Leeuw, D. M. *Phys. Rev. Lett.* **2003**, *91*, 216601.
(67) Warta, W.; Stehle, R.; Karl, N. *Appl. Phys. A: Mater. Sci. Process.* **1985**, *36*, 163.
(68) Ostroverkhova, O.; Cooke, D. G.; Shcherbyna, S.; Egerton, R. F.; Hegmann, F. A.; Tykwinski, R. R.; Anthony, J. E. *Phys. Rev. B* **2005**, *71*, 035204.
(69) Ostroverkhova, O.; Cooke, D. G.; Hegmann, F. A.; Anthony, J. E.; Podzorov, V.; Gershenson, M. E.; Jurchescu, O. D.; Palstra, T. T. M. *Appl. Phys. Lett.* **2006**, *88*, 162101.
(70) Podzorov, V.; Menard, E.; Borissov, A.; Kiryukhin, V.; Rogers, J. A.; Gershenson, M. E. *Phys. Rev. Lett.* **2004**, *93*, 086602.
(71) Podzorov, V.; Menard, E.; Rogers, J. A.; Gershenson, M. E. *Phys. Rev. Lett.* **2005**, *95*, 226601.
(72) Cheng, Y. C.; Silbey, R. J.; da Silva, D. A.; Calbert, J. P.; Cornil, J.; Bredas, J. L. *J. Chem. Phys.* **2003**, *118*, 3764.
(73) Kenkre, V. M. *Phys. Lett. A* **2002**, *305*, 443.
(74) Troisi, A.; Orlandi, G. *J. Phys. Chem. A* **2006**, *110*, 4065.
(75) Troisi, A.; Orlandi, G. *Phys. Rev. Lett.* **2006**, *96*, 086601.
(76) Hulea, I. N.; Fratini, S.; Xie, H.; Mulder, C. L.; Iossad, N. N.; Rastelli, G.; Ciuchi, S.; Morpurgo, A. F. *Nat. Mater.* **2006**, *5*, 982.
(77) Horowitz, G. *J. Mater. Res.* **2004**, *19*, 1946.
(78) Sirringhaus, H. *Adv. Mater.* **2005**, *17*, 2411.
(79) Salleo, A.; Chen, T. W.; Volkel, A. R.; Wu, Y.; Liu, P.; Ong, B. S.; Street, R. A. *Phys. Rev. B* **2004**, *70*, 115311.
(80) Bredas, J. L.; Beljonne, D.; Coropceanu, V.; Cornil, J. *Chem. Rev.* **2004**, *104*, 4971.
(81) Cornil, J.; Gueli, I.; Dkhissi, A.; Sancho-Garcia, J. C.; Hennebicq, E.; Calbert, J. P.; Lemaur, V.; Beljonne, D.; Bredas, J. L. *J. Chem. Phys.* **2003**, *118*, 6615.
(82) Nakayama, K.; Umehara, M.; Yokoyama, M. *Jpn. J. Appl. Phys.* **2006**, *45*, 974.
(83) Schroeder, R.; Majewski, L. A.; Grell, M. *Appl. Phys. Lett.* **2004**, *84*, 1004.
(84) Tsukagoshi, K.; Shigeto, K.; Yagi, I.; Aoyagi, Y. *Appl. Phys. Lett.* **2006**, *89*, Art. No. 113507.
(85) Ishii, H.; Sugiyama, K.; Ito, E.; Seki, K. *Adv. Mater.* **1999**, *11*, 605.
(86) Burgi, L.; Richards, T. J.; Friend, R. H.; Sirringhaus, H. *J. Appl. Phys.* **2003**, *94*, 6129.
(87) Pesavento, P. V.; Chesterfield, R. J.; Newman, C. R.; Frisbie, C. D. *J. Appl. Phys.* **2004**, *96*, 7312.
(88) Kanicki, J.; Libsch, F. R.; Griffith, J.; Polastre, R. *J. Appl. Phys.* **1991**, *69*, 2339.
(89) Zaumseil, J.; Baldwin, K. W.; Rogers, J. A. *J. Appl. Phys.* **2003**, *93*, 6117.
(90) Anthopoulos, T. D.; de Leeuw, D. M.; Cantatore, E.; van't Hof, P.; Alma, J.; Hummelen, J. C. *J. Appl. Phys.* **2005**, *98*, 054503.
(91) Hamadani, B. H.; Natelson, D. *Appl. Phys. Lett.* **2004**, *84*, 443.
(92) Wan, A.; Hwang, J.; Amy, F.; Kahn, A. *Org. Electron.* **2005**, *6*, 47.
(93) Vazquez, H.; Oszwaldowski, R.; Pou, P.; Ortega, J.; Perez, R.; Flores, F.; Kahn, A. *Europhys. Lett.* **2004**, *65*, 802.
(94) de Boer, B.; Hadipour, A.; Mandoc, M. M.; van Woudenbergh, T.; Blom, P. W. M. *Adv. Mater.* **2005**, *17*, 621.
(95) Hamadani, B. H.; Corley, D. A.; Ciszek, J. W.; Tour, J. M.; Natelson, D. *Nano Lett.* **2006**, *6*, 1303.
(96) Abkowitz, M. A.; Mizes, H. A. *Appl. Phys. Lett.* **1995**, *66*, 1288.
(97) Conwell, E. M.; Wu, M. W. *Appl. Phys. Lett.* **1997**, *70*, 1867.
(98) Arkhipov, V. I.; Emelianova, E. V.; Tak, Y. H.; Bassler, H. *J. Appl. Phys.* **1998**, *84*, 848.
(99) Scott, J. C.; Malliaras, G. G. *Chem. Phys. Lett.* **1999**, *299*, 115.
(100) Shen, Y. L.; Hosseini, A. R.; Wong, M. H.; Malliaras, G. G. *ChemPhysChem* **2004**, *5*, 16.
(101) Kahn, A.; Koch, N.; Gao, W. Y. *J. Polym. Sci., B: Polym. Phys.* **2003**, *41*, 2529.
(102) Lin, Y. Y.; Gundlach, D. J.; Nelson, S. F.; Jackson, T. N. *IEEE Electron Device Lett.* **1997**, *18*, 606.
(103) Sirringhaus, H.; Brown, P. J.; Friend, R. H.; Nielsen, M. M.; Bechgaard, K.; Langeveld-Voss, B. M. W.; Spiering, A. J. H.; Janssen, R. A. J.; Meijer, E. W.; Herwig, P.; de Leeuw, D. M. *Nature* **1999**, *401*, 685.
(104) Salleo, A.; Chabinyc, M. L.; Yang, M. S.; Street, R. A. *Appl. Phys. Lett.* **2002**, *81*, 4383.

(105) Shtein, M.; Mapel, J.; Benziger, J. B.; Forrest, S. R. *Appl. Phys. Lett.* **2002**, *81*, 268.
(106) Lee, J.; Kim, J. H.; Im, S. *Appl. Phys. Lett.* **2003**, *83*, 2689.
(107) Majewski, L. A.; Grell, M.; Ogier, S. D.; Veres, J. *Org. Electron.* **2003**, *4*, 27.
(108) Bartic, C.; Jansen, H.; Campitelli, A.; Borghs, S. *Org. Electron.* **2002**, *3*, 65.
(109) Peng, X. Z.; Horowitz, G.; Fichou, D.; Garnier, F. *Appl. Phys. Lett.* **1990**, *57*, 2013.
(110) Bao, Z. N.; Kuck, V.; Rogers, J. A.; Paczkowski, M. A. *Adv. Funct. Mater.* **2002**, *12*, 526.
(111) Dimitrakopoulos, C. D.; Furman, B. K.; Graham, T.; Hegde, S.; Purushothaman, S. *Synth. Met.* **1998**, *92*, 47.
(112) Klauk, H.; Halik, M.; Zschieschang, U.; Schmid, G.; Radlik, W.; Weber, W. *J. Appl. Phys.* **2002**, *92*, 5259.
(113) Nunes, G.; Zane, S. G.; Meth, J. S. *J. Appl. Phys.* **2005**, *98*, 104503.
(114) Lee, S.; Koo, B.; Shin, J.; Lee, E.; Park, H.; Kim, H. *Appl. Phys. Lett.* **2006**, *88*, 162109.
(115) Veres, J.; Ogier, S. D.; Leeming, S. W.; Cupertino, D. C.; Khaffaf, S. M. *Adv. Funct. Mater.* **2003**, *13*, 199.
(116) Stassen, A. F.; de Boer, R. W. I.; Iosad, N. N.; Morpurgo, A. F. *Appl. Phys. Lett.* **2004**, *85*, 3899.
(117) Afzali, A.; Dimitrakopoulos, C. D.; Breen, T. L. *J. Am. Chem. Soc.* **2002**, *124*, 8812.
(118) Afzali, A.; Kagan, C. R.; Traub, G. P. *Synth. Met.* **2005**, *155*, 490.
(119) Anthony, J. E.; Brooks, J. S.; Eaton, D. L.; Parkin, S. R. *J. Am. Chem. Soc.* **2001**, *123*, 9482.
(120) Payne, M. M.; Parkin, S. R.; Anthony, J. E.; Kuo, C. C.; Jackson, T. N. *J. Am. Chem. Soc.* **2005**, *127*, 4986.
(121) Dickey, K. C.; Anthony, J. E.; Loo, Y. L. *Adv. Mater.* **2006**, *18*, 1721.
(122) Anthony, J. E. *Chem. Rev.* **2006**, *106*, 5028.
(123) Chang, J. F.; Sun, B. Q.; Breiby, D. W.; Nielsen, M. M.; Solling, T. I.; Giles, M.; McCulloch, I.; Sirringhaus, H. *Chem. Mat.* **2004**, *16*, 4772.
(124) Kline, R. J.; McGehee, M. D.; Kadnikova, E. N.; Liu, J. S.; Frechet, J. M. J.; Toney, M. F. *Macromolecules* **2005**, *38*, 3312.
(125) Ong, B. S.; Wu, Y. L.; Liu, P.; Gardner, S. *J. Am. Chem. Soc.* **2004**, *126*, 3378.
(126) Heeney, M.; Bailey, C.; Genevicius, K.; Shkunov, M.; Sparrowe, D.; Tierney, S.; McCulloch, I. *J. Am. Chem. Soc.* **2005**, *127*, 1078.
(127) McCulloch, I.; Heeney, M.; Bailey, C.; Genevicius, K.; Macdonald, I.; Shkunov, M.; Sparrowe, D.; Tierney, S.; Wagner, R.; Zhang, W. M.; Chabinyc, M. L.; Kline, R. J.; McGehee, M. D.; Toney, M. F. *Nat. Mater.* **2006**, *5*, 328.
(128) de Boer, R. W. I.; Gershenson, M. E.; Morpurgo, A. F.; Podzorov, V. *Phys. Status Solidi A: Appl. Res.* **2004**, *201*, 1302.
(129) Kloc, C.; Simpkins, P. G.; Siegrist, T.; Laudise, R. A. *J. Cryst. Growth* **1997**, *182*, 416.
(130) Laudise, R. A.; Kloc, C.; Simpkins, P. G.; Siegrist, T. *J. Cryst. Growth* **1998**, *187*, 449.
(131) Butko, V. Y.; Chi, X.; Lang, D. V.; Ramirez, A. P. *Appl. Phys. Lett.* **2003**, *83*, 4773.
(132) Butko, V. Y.; Chi, X.; Ramirez, A. P. *Solid State Commun.* **2003**, *128*, 431.
(133) Podzorov, V.; Pudalov, V. M.; Gershenson, M. E. *Appl. Phys. Lett.* **2003**, *82*, 1739.
(134) Mas-Torrent, M.; Hadley, P.; Bromley, S. T.; Crivillers, N.; Veciana, J.; Rovira, C. *Appl. Phys. Lett.* **2005**, *86*, 012110.
(135) Mas-Torrent, M.; Hadley, P.; Bromley, S. T.; Ribas, X.; Tarres, J.; Mas, M.; Molins, E.; Veciana, J.; Rovira, C. *J. Am. Chem. Soc.* **2004**, *126*, 8546.
(136) Mas-Torrent, M.; Hadley, P.; Ribas, X.; Rovira, C. *Synth. Met.* **2004**, *146*, 265.
(137) Briseno, A. L.; Roberts, M.; Ling, M. M.; Moon, H.; Nemanick, E. J.; Bao, Z. N. *J. Am. Chem. Soc.* **2006**, *128*, 3880.
(138) da Silva, D. A.; Kim, E. G.; Bredas, J. L. *Adv. Mater.* **2005**, *17*, 1072.
(139) Menard, E.; Podzorov, V.; Hur, S. H.; Gaur, A.; Gershenson, M. E.; Rogers, J. A. *Adv. Mater.* **2004**, *16*, 2097.
(140) Takeya, J.; Tsukagoshi, K.; Aoyagi, Y.; Takenobu, T.; Iwasa, Y. *Jpn. J. Appl. Phys.* **2005**, *44*, 1393.
(141) Sundar, V. C.; Zaumseil, J.; Podzorov, V.; Menard, E.; Willett, R. L.; Someya, T.; Gershenson, M. E.; Rogers, J. A. *Science* **2004**, *303*, 1644.
(142) Lee, J. Y.; Roth, S.; Park, Y. W. *Appl. Phys. Lett.* **2006**, *88*, 252106.
(143) Troisi, A.; Orlandi, G.; Anthony, J. E. *Chem. Mat.* **2005**, *17*, 5024.
(144) Bromley, S. T.; Mas-Torrent, M.; Hadley, P.; Rovira, C. *J. Am. Chem. Soc.* **2004**, *126*, 6544.
(145) Brown, A. R.; Pomp, A.; Hart, C. M.; Deleeuw, D. M. *Science* **1995**, *270*, 972.
(146) Brown, A. R.; Jarrett, C. P.; deLeeuw, D. M.; Matters, M. *Synth. Met.* **1997**, *88*, 37.
(147) Stingelin-Stutzmann, N.; Smits, E.; Wondergem, H.; Tanase, C.; Blom, P.; Smith, P.; de Leeuw, D. *Nat. Mater.* **2005**, *4*, 601.
(148) Klauk, H.; Gundlach, D. J.; Jackson, T. N. *IEEE Electron Device Lett.* **1999**, *20*, 289.
(149) Gelinck, G. H.; Geuns, T. C. T.; de Leeuw, D. M. *Appl. Phys. Lett.* **2000**, *77*, 1487.
(150) Klauk, H.; Halik, M.; Zschieschang, U.; Eder, F.; Schmid, G.; Dehm, C. *Appl. Phys. Lett.* **2003**, *82*, 4175.
(151) de Vusser, S.; Genoe, J.; Heremans, P. *IEEE Trans. Electron Devices* **2006**, *53*, 601.
(152) Dodabalapur, A.; Laquindanum, J.; Katz, H. E.; Bao, Z. *Appl. Phys. Lett.* **1996**, *69*, 4227.
(153) Yoo, B.; Jung, T.; Basu, D.; Dodabalapur, A.; Jones, B. A.; Facchetti, A.; Wasielewski, M. R.; Marks, T. J. *Appl. Phys. Lett.* **2006**, *88*, 082104.
(154) Crone, B.; Dodabalapur, A.; Lin, Y. Y.; Filas, R. W.; Bao, Z.; LaDuca, A.; Sarpeshkar, R.; Katz, H. E.; Li, W. *Nature* **2000**, *403*, 521.
(155) Loo, Y. L.; Willett, R. L.; Baldwin, K. W.; Rogers, J. A. *Appl. Phys. Lett.* **2002**, *81*, 562.
(156) Sakamoto, Y.; Suzuki, T.; Kobayashi, M.; Gao, Y.; Fukai, Y.; Inoue, Y.; Sato, F.; Tokito, S. *J. Am. Chem. Soc.* **2004**, *126*, 8138.
(157) Gundlach, D. J.; Pernstich, K. P.; Wilckens, G.; Gruter, M.; Haas, S.; Batlogg, B. *J. Appl. Phys.* **2005**, *98*, 064502.
(158) Kanbara, T.; Shibata, K.; Fujiki, S.; Kubozono, Y.; Kashino, S.; Urisu, T.; Sakai, M.; Fujiwara, A.; Kumashiro, R.; Tanigaki, K. *Chem. Phys. Lett.* **2003**, *379*, 223.
(159) Yoon, M. H.; Yan, H.; Facchetti, A.; Marks, T. J. *J. Am. Chem. Soc.* **2005**, *127*, 10388.
(160) Lin, Y. Y.; Dodabalapur, A.; Sarpeshkar, R.; Bao, Z.; Li, W.; Baldwin, K.; Raju, V. R.; Katz, H. E. *Appl. Phys. Lett.* **1999**, *74*, 2714.
(161) Newman, C. R.; Frisbie, C. D.; da Silva, D. A.; Bredas, J. L.; Ewbank, P. C.; Mann, K. R. *Chem. Mater.* **2004**, *16*, 4436.
(162) deLeeuw, D. M.; Simenon, M. M. J.; Brown, A. R.; Einerhand, R. E. F. *Synth. Met.* **1997**, *87*, 53.
(163) Kobayashi, S.; Takenobu, T.; Mori, S.; Fujiwara, A.; Iwasa, Y. *Appl. Phys. Lett.* **2003**, *82*, 4581.
(164) Waldauf, C.; Schilinsky, P.; Perisutti, M.; Hauch, J.; Brabec, C. J. *Adv. Mater.* **2003**, *15*, 2084.
(165) Chikamatsu, M.; Nagamatsu, S.; Yoshida, Y.; Saito, K.; Yase, K.; Kikuchi, K. *Appl. Phys. Lett.* **2005**, *87*, 203504.
(166) Bao, Z. A.; Lovinger, A. J.; Brown, J. *J. Am. Chem. Soc.* **1998**, *120*, 207.
(167) Jones, B. A.; Ahrens, M. J.; Yoon, M. H.; Facchetti, A.; Marks, T. J.; Wasielewski, M. R. *Angew. Chem., Int. Ed.* **2004**, *43*, 6363.
(168) Facchetti, A.; Mushrush, M.; Katz, H. E.; Marks, T. J. *Adv. Mater.* **2003**, *15*, 33.
(169) Facchetti, A.; Yoon, M. H.; Stern, C. L.; Katz, H. E.; Marks, T. J. *Angew. Chem., Int. Ed.* **2003**, *42*, 3900.
(170) Yoon, M. H.; Facchetti, A.; Stern, C. E.; Marks, T. J. *J. Am. Chem. Soc.* **2006**, *128*, 5792.
(171) Babel, A.; Jenekhe, S. A. *J. Am. Chem. Soc.* **2003**, *125*, 13656.
(172) Kim, J. S.; Ho, P. K. H.; Murphy, C. E.; Friend, R. H. *Macromolecules* **2004**, *37*, 2861.
(173) Corcoran, N.; Arias, A. C.; Kim, J. S.; MacKenzie, J. D.; Friend, R. H. *Appl. Phys. Lett.* **2003**, *82*, 299.
(174) Xia, Y. J.; Friend, R. H. *Macromolecules* **2005**, *38*, 6466.
(175) Kim, Y.; Cook, S.; Choulis, S. A.; Nelson, J.; Durrant, J. R.; Bradley, D. D. C. *Chem. Mater.* **2004**, *16*, 4812.
(176) Snaith, H. J.; Arias, A. C.; Morteani, A. C.; Silva, C.; Friend, R. H. *Nano Lett.* **2002**, *2*, 1353.
(177) Arias, A. C.; Corcoran, N.; Banach, M.; Friend, R. H.; MacKenzie, J. D.; Huck, W. T. S. *Appl. Phys. Lett.* **2002**, *80*, 1695.
(178) Yasuda, T.; Fujita, K.; Tsutsui, T. *Jpn. J. Appl. Phys.* **2004**, *43*, 7731.
(179) Yasuda, T.; Goto, T.; Fujita, K.; Tsutsui, T. *Appl. Phys. Lett.* **2004**, *85*, 2098.
(180) Singh, T. B.; Meghdadi, T.; Gunes, S.; Marjanovic, N.; Horowitz, G.; Lang, P.; Bauer, S.; Sariciftci, N. S. *Adv. Mater.* **2005**, *17*, 2315.
(181) Benson, N.; Schidleja, M.; Melzer, C.; Schmechel, R.; von Seggern, H. *Appl. Phys. Lett.* **2006**, *89*, Art. No. 182105.
(182) Yoon, M. H.; Kim, C.; Facchetti, A.; Marks, T. J. *J. Am. Chem. Soc.* **2006**, *128*, 12851.
(183) Schmechel, R.; Ahles, M.; von Seggern, H. *J. Appl. Phys.* **2005**, *98*, 084511.
(184) Paasch, G.; Lindner, T.; Rost-Bietsch, C.; Karg, S.; Riess, W.; Scheinert, S. *J. Appl. Phys.* **2005**, *98*, 084505.
(185) Smith, D. L.; Ruden, P. P. *Appl. Phys. Lett.* **2006**, *89*, Art. No. 233519.
(186) Neudeck, G. W.; Malhotra, A. K. *J. Appl. Phys.* **1975**, *46*, 239.
(187) Pfleiderer, H.; Kusian, W. *Solid-State Electron.* **1986**, *29*, 317.
(188) Pfleiderer, H. *IEEE Trans. Electron Devices* **1986**, *33*, 145.
(189) Hack, M.; Shur, M.; Czubatyj, W. *Appl. Phys. Lett.* **1986**, *48*, 1386.

(190) Street, R. A.; Clarke, D. R.; Suresh, S. *Hydrogenated Amorphous Silicon*; Cambridge University Press: Cambridge, U.K., 2005.
(191) Vanberkel, C.; Powell, M. J. *Appl. Phys. Lett*. **1987**, *51*, 1094.
(192) Chiang, C. S.; Kanicki, J.; Takechi, K. *Jpn. J. Appl. Phys*. **1998**, *37*, 4704.
(193) Avouris, P. *Acc. Chem. Res*. **2002**, *35*, 1026.
(194) Tans, S. J.; Verschueren, A. R. M.; Dekker, C. *Nature* **1998**, *393*, 49.
(195) Chen, Z. H.; Appenzeller, J.; Lin, Y. M.; Sippel-Oakley, J.; Rinzler, A. G.; Tang, J. Y.; Wind, S. J.; Solomon, P. M.; Avouris, P. *Science* **2006**, *311*, 1735.
(196) Martel, R.; Derycke, V.; Lavoie, C.; Appenzeller, J.; Chan, K. K.; Tersoff, J.; Avouris, P. *Phys. Rev. Lett.* **2001**, *87*.
(197) Misewich, J. A.; Martel, R.; Avouris, P.; Tsang, J. C.; Heinze, S.; Tersoff, J. *Science* **2003**, *300*, 783.
(198) Freitag, M.; Chen, J.; Tersoff, J.; Tsang, J. C.; Fu, Q.; Liu, J.; Avouris, P. *Phys. Rev. Lett.* **2004**, *93*, 076803.
(199) Dodabalapur, A.; Katz, H. E.; Torsi, L.; Haddon, R. C. *Science* **1995**, *269*, 1560.
(200) Dodabalapur, A.; Katz, H. E.; Torsi, L.; Haddon, R. C. *Appl. Phys. Lett*. **1996**, *68*, 1108.
(201) Rost, C.; Gundlach, D. J.; Karg, S.; Riess, W. *J. Appl. Phys*. **2004**, *95*, 5782.
(202) Kuwahara, E.; Kusai, H.; Nagano, T.; Takayanagi, T.; Kubozono, Y. *Chem. Phys. Lett.* **2005**, *413*, 379.
(203) Kang, S. J.; Yi, Y.; Kim, C. Y.; Cho, K.; Seo, J. H.; Noh, M.; Jeong, K.; Yoo, K. H.; Whang, C. N. *Appl. Phys. Lett*. **2005**, *87*, 233502.
(204) Dinelli, F.; Capelli, R.; Loi, M. A.; Murgia, M.; Muccini, M.; Facchetti, A.; Marks, T. J. *Adv. Mater*. **2006**, *18*, 1416.
(205) Wang, J.; Wang, H. B.; Yan, X. J.; Huang, H. C.; Yan, D. H. *Appl. Phys. Lett*. **2005**, *87*, 093507.
(206) Wang, J.; Wang, H. B.; Yan, X. J.; Huang, H. C.; Yan, D. H. *Chem. Phys. Lett.* **2005**, *407*, 87.
(207) Ye, R.; Baba, M.; Mori, K. *Jpn. J. Appl. Phys.* **2005**, *44*, 581.
(208) Ye, R. B.; Baba, M.; Oishi, Y.; Mori, K.; Suzuki, K. *Appl. Phys. Lett.* **2005**, *86*, 253505.
(209) Wang, J.; Wang, H. B.; Yan, X. J.; Huang, H. C.; Jin, D.; Shi, J. W.; Tang, Y. H.; Yan, D. H. *Adv. Funct. Mater*. **2006**, *16*, 824.
(210) Wang, H. B.; Wang, J.; Yan, X. J.; Shi, J. W.; Tian, H. K.; Geng, Y. H.; Yan, D. H. *Appl. Phys. Lett.* **2006**, *88*, 133508.
(211) Rost, C.; Karg, S.; Riess, W.; Loi, M. A.; Murgia, M.; Muccini, M. *Appl. Phys. Lett.* **2004**, *85*, 1613.
(212) Loi, M. A.; Rost-Bietsch, C.; Murgia, M.; Karg, S.; Riess, W.; Muccini, M. *Adv. Funct. Mater.* **2006**, *16*, 41.
(213) Unni, K. N. N.; Pandey, A. K.; Alem, S.; Nunzi, J. M. *Chem. Phys. Lett.* **2006**, *421*, 554.
(214) Inoue, Y.; Sakamoto, Y.; Suzuki, T.; Kobayashi, M.; Gao, Y.; Tokito, S. *Jpn. J. Appl. Phys.* **2005**, *44*, 3663.
(215) Tada, K.; Harada, H.; Yoshino, K. *Jpn. J. Appl. Phys.* **1996**, *35*, L944.
(216) Meijer, E. J.; de Leeuw, D. M.; Setayesh, S.; van Veenendaal, E.; Huisman, B. H.; Blom, P. W. M.; Hummelen, J. C.; Scherf, U.; Klapwijk, T. M. *Nat. Mater.* **2003**, *2*, 678.
(217) Singh, T. B.; Gunes, S.; Marjanovic, N.; Sariciftci, N. S.; Menon, R. *J. Appl. Phys.* **2005**, *97*, 114508.
(218) Hayashi, Y.; Kanamori, H.; Yamada, I.; Takasu, A.; Takagi, S.; Kaneko, K. *Appl. Phys. Lett.* **2005**, *86*, 052104.
(219) Babel, A.; Wind, J. D.; Jenekhe, S. A. *Adv. Funct. Mater.* **2004**, *14*, 891.
(220) Cho, S. N.; Yuen, J.; Kim, J. Y.; Lee, K.; Heeger, A. J. *Appl. Phys. Lett.* **2006**, *89*, Art. No. 153505.
(221) Shkunov, M.; Simms, R.; Heeney, M.; Tierney, S.; McCulloch, I. *Adv. Mater.* **2005**, *17*, 2608.
(222) Anthopoulos, T. D.; Tanase, C.; Setayesh, S.; Meijer, E. J.; Hummelen, J. C.; Blom, P. W. M.; de Leeuw, D. M. *Adv. Mater*. **2004**, *16*, 2174.
(223) Anthopoulos, T. D.; de Leeuw, D. M.; Cantatore, E.; Setayesh, S.; Meijer, E. J.; Tanase, C.; Hummelen, J. C.; Blom, P. W. M. *Appl. Phys. Lett.* **2004**, *85*, 4205.
(224) Anthopoulos, T. D.; Kooistra, F. B.; Wondergem, H. J.; Kronholm, D.; Hummelen, J. C.; de Leeuw, D. M. *Adv. Mater*. **2006**, *18*, 1679.
(225) Kunugi, Y.; Takimiya, K.; Negishi, N.; Otsubo, T.; Aso, Y. *J. Mater. Chem.* **2004**, *14*, 2840.
(226) Amriou, S.; Mehta, A.; Bryce, M. R. *J. Mater. Chem.* **2005**, *15*, 1232.
(227) Takahashi, T.; Takenobu, T.; Takeya, J.; Iwasa, Y. *Appl. Phys. Lett.* **2006**, *88*, 033505.
(228) Seo, S.; Park, B. M.; Evans, P. G. *Appl. Phys. Lett.* **2006**, *88*, 232114.
(229) de Boer, R. W. I.; Stassen, A. F.; Craciun, M. F.; Mulder, C. L.; Molinari, A.; Rogge, S.; Morpurgo, A. F. *Appl. Phys. Lett.* **2005**, *86*, 262109.
(230) Yasuda, T.; Tsutsui, T. *Chem. Phys. Lett.* **2005**, *402*, 395.
(231) Goldmann, C.; Haas, S.; Krellner, C.; Pernstich, K. P.; Gundlach, D. J.; Batlogg, B. *J. Appl. Phys.* **2004**, *96*, 2080.
(232) Yasuda, T.; Goto, T.; Fujita, K.; Tsutsui, T. *Mol. Cryst. Liq. Cryst.* **2006**, *444*, 219.
(233) Singh, T. B.; Senkarabacak, P.; Sariciftci, N. S.; Tanda, A.; Lackner, C.; Hagelauer, R.; Horowitz, G. *Appl. Phys. Lett.* **2006**, *89*, 033512.
(234) Reisch, H.; Wiesler, U.; Scherf, U.; Tuytuylkov, N. *Macromolecules* **1996**, *29*, 8204.
(235) Chesterfield, R. J.; Newman, C. R.; Pappenfus, T. M.; Ewbank, P. C.; Haukaas, M. H.; Mann, K. R.; Miller, L. L.; Frisbie, C. D. *Adv. Mater.* **2003**, *15*, 1278.
(236) Nishikawa, T.; Kobayashi, S.; Nakanowatari, T.; Mitani, T.; Shimoda, T.; Kubozono, Y.; Yamamoto, G.; Ishii, H.; Niwano, M.; Iwasa, Y. *J. Appl. Phys.* **2005**, *97*, 104509.
(237) Tada, H.; Touda, H.; Takada, M.; Matsushige, K. *Appl. Phys. Lett.* **2000**, *76*, 873.
(238) Yasuda, T.; Tsutsui, T. *Jpn. J. Appl. Phys.* **2006**, *45*, L595.
(239) Anthopoulos, T. D.; Setayesh, S.; Smits, E.; Coelle, M.; Cantatore, E.; Blom, P. W. M.; de Leeuw, D. M. *Adv. Mater.* **2006**, *18*, 1900.
(240) Smits, E. C. P.; Anthopoulos, T. D.; Setayesh, S.; van Veenendaal, E.; Coehoorn, R.; Blom, P. W. M.; de Boer, B.; de Leeuw, D. M. *Phys. Rev. B* **2006**, *73*, 205316.
(241) Ahles, M.; Schmechel, R.; von Seggern, H. *Appl. Phys. Lett.* **2004**, *85*, 4499.
(242) Yamamoto, T.; Yasuda, T.; Sakai, Y.; Aramaki, S.; Ramaw, A. *Macromol. Rapid Commun.* **2005**, *26*, 1214.
(243) Zaumseil, J. Unpublished results.
(244) Choulis, S. A.; Kim, Y.; Nelson, J.; Bradley, D. D. C.; Giles, M.; Shkunov, M.; McCulloch, I. *Appl. Phys. Lett.* **2004**, *85*, 3890.
(245) Zaumseil, J.; Friend, R. H.; Sirringhaus, H. *Nat. Mater*. **2006**, *5*, 69.
(246) Swensen, J. S.; Soci, C.; Heeger, A. J. *Appl. Phys. Lett.* **2005**, *87*, 253511.
(247) Zaumseil, J.; Donley, C. L.; Kim, J. S.; Friend, R. H.; Sirringhaus, H. *Adv. Mater*. **2006**, *18*, 2708.
(248) Yoon, M. H.; DiBenedetto, S. A.; Facchetti, A.; Marks, T. J. *J. Am. Chem. Soc*. **2005**, *127*, 1348.
(249) Verlaak, S.; Cheyns, D.; Debucquoy, M.; Arkhipov, V.; Heremans, P. *Appl. Phys. Lett.* **2004**, *85*, 2405.
(250) Walters, R. J.; Bourianoff, G. I.; Atwater, H. A. *Nat. Mater*. **2005**, *4*, 143.
(251) Saito, S.; Hisamoto, D.; Shimizu, H.; Hamamura, H.; Tsuchiya, R.; Matsui, Y.; Mine, T.; Arai, T.; Sugii, N.; Torii, K.; Kimura, S.; Onai, T. *Appl. Phys. Lett.* **2006**, *89*, Art. No. 163504.
(252) Feng, M.; Holonyak, N.; Chan, R. *Appl. Phys. Lett.* **2004**, *84*, 1952.
(253) Tang, C. W.; Vanslyke, S. A. *Appl. Phys. Lett.* **1987**, *51*, 913.
(254) Friend, R. H.; Gymer, R. W.; Holmes, A. B.; Burroughes, J. H.; Marks, R. N.; Taliani, C.; Bradley, D. D. C.; Dos Santos, D. A.; Bredas, J. L.; Logdlund, M.; Salaneck, W. R. *Nature* **1999**, *397*, 121.
(255) D'Andrade, B. W.; Forrest, S. R. *Adv. Mater*. **2004**, *16*, 1585.
(256) Burroughes, J. H.; Bradley, D. D. C.; Brown, A. R.; Marks, R. N.; Mackay, K.; Friend, R. H.; Burns, P. L.; Holmes, A. B. *Nature* **1990**, *347*, 539.
(257) Dodabalapur, A.; Katz, H. E.; Torsi, L. *Adv. Mater*. **1996**, *8*, 853.
(258) Hepp, A.; Heil, H.; Weise, W.; Ahles, M.; Schmechel, R.; von Seggern, H. *Phys. Rev. Lett.* **2003**, *91*, 157406.
(259) Ahles, M.; Hepp, A.; Schmechel, R.; von Seggern, H. *Appl. Phys. Lett*. **2004**, *84*, 428.
(260) Santato, C.; Capelli, R.; Loi, M. A.; Murgia, M.; Cicoira, F.; Roy, V. A. L.; Stallinga, P.; Zamboni, R.; Rost, C.; Karg, S. E.; Muccini, M. *Synth. Met.* **2004**, *146*, 329.
(261) Cicoira, F.; Santato, C.; Melucci, M.; Favaretto, L.; Gazzano, M.; Muccini, M.; Barbarella, G. *Adv. Mater*. **2006**, *18*, 169.
(262) Santato, C.; Manunza, I.; Bonfiglio, A.; Cicoira, F.; Cosseddu, P.; Zamboni, R.; Muccini, M. *Appl. Phys. Lett.* **2005**, *86*, 141106.
(263) Santato, C.; Cicoira, F.; Cosseddu, P.; Bonfiglio, A.; Bellutti, P.; Muccini, M.; Zamboni, R.; Rosei, F.; Mantoux, A.; Doppelt, P. *Appl. Phys. Lett.* **2006**, *88*, 163511.
(264) Sakanoue, T.; Fujiwara, E.; Yamada, R.; Tada, H. *Chem. Lett.* **2005**, *34*, 494.
(265) Oyamada, T.; Uchiuzou, H.; Sasabe, H.; Adachi, C. *J. Soc. Inf. Disp.* **2005**, *13*, 869.
(266) Oyamada, T.; Uchiuzou, H.; Akiyama, S.; Oku, Y.; Shimoji, N.; Matsushige, K.; Sasabe, H.; Adachi, C. *J. Appl. Phys.* **2005**, *98*, 074506.
(267) Oyamada, T.; Sasabe, H.; Adachi, C.; Okuyama, S.; Shimoji, N.; Matsushige, K. *Appl. Phys. Lett.* **2005**, *86*, 093505.
(268) Nakamura, K.; Ichikawa, M.; Fushiki, R.; Kamikawa, T.; Inoue, M.; Koyama, T.; Taniguchi, Y. *Jpn. J. Appl. Phys.* **2005**, *44*, 1367.
(269) Sakanoue, T.; Fujiwara, E.; Yamada, R.; Tada, H. *Appl. Phys. Lett.* **2004**, *84*, 3037.

(270) Swensen, J.; Moses, D.; Heeger, A. J. *Synth. Met.* **2005**, *153*, 53.
(271) Reynaert, J.; Cheyns, D.; Janssen, D.; Muller, R.; Arkhipov, V. I.; Genoe, J.; Borghs, G.; Heremans, P. *J. Appl. Phys.* **2005**, *97*, 114501.
(272) de Vusser, S.; Schols, S.; Steudel, S.; Verlaak, S.; Genoe, J.; Oosterbaan, W. D.; Lutsen, L. J.; Vanderzande, D. J.; Heremans, M. P. *Appl. Phys. Lett.* **2006**, *89*, Art. No. 223504.
(273) Ho, P. K. H.; Kim, J. S.; Burroughes, J. H.; Becker, H.; Li, S. F. Y.; Brown, T. M.; Cacialli, F.; Friend, R. H. *Nature* **2000**, *404*, 481.
(274) Kim, J. S.; Ho, P. K. H.; Greenham, N. C.; Friend, R. H. *J. Appl. Phys.* **2000**, *88*, 1073.
(275) Donley, C. L.; Zaumseil, J.; Andreasen, J. W.; Nielsen, M. M.; Sirringhaus, H.; Friend, R. H.; Kim, J. S. *J. Am. Chem. Soc.* **2005**, *127*, 12890.
(276) Baldo, M. A.; Holmes, R. J.; Forrest, S. R. *Phys. Rev. B* **2002**, *66*, Art. No. 035321.
(277) Tessler, N.; Pinner, D. J.; Cleave, V.; Ho, P. K. H.; Friend, R. H.; Yahioglu, G.; Barny, P. L.; Gray, J.; de Souza, M.; Rumbles, G. *Synth. Met.* **2000**, *115*, 57.

CR0501543